Cell

Competing E3 Ubiquitin Ligases Govern Circadian Periodicity by Degradation of CRY in Nucleus and Cytoplasm

Seung-Hee Yoo,[1,2] Jennifer A. Mohawk,[1,2,7] Sandra M. Siepka,[4,7] Yongli Shan,[1] Seong Kwon Huh,[1] Hee-Kyung Hong,[4] Izabela Kornblum,[2] Vivek Kumar,[1,2] Nobuya Koike,[1] Ming Xu,[3] Justin Nussbaum,[5] Xinran Liu,[1,8] Zheng Chen,[6] Zhijian J. Chen,[2,3] Carla B. Green,[1,5] and Joseph S. Takahashi[1,2,*]

[1]Department of Neuroscience
[2]Howard Hughes Medical Institute
[3]Department of Molecular Biology
University of Texas Southwestern Medical Center, Dallas, TX 75390, USA
[4]Department of Neurobiology, Northwestern University, 2205 Tech Drive, Evanston, IL 60208, USA
[5]Department of Biology, University of Virginia, Charlottesville, VA 22904, USA
[6]Department of Biochemistry and Molecular Biology, University of Texas Health Science Center at Houston, Houston, TX 77030, USA
[7]These authors contributed equally to this work
[8]Present address: Department of Cell Biology, Yale University School of Medicine, 333 Cedar Street, New Haven, CT 06520 USA
*Correspondence: joseph.takahashi@utsouthwestern.edu
http://dx.doi.org/10.1016/j.cell.2013.01.055

SUMMARY

Period determination in the mammalian circadian clock involves the turnover rate of the repressors CRY and PER. We show that CRY ubiquitination engages two competing E3 ligase complexes that either lengthen or shorten circadian period in mice. Cloning of a short-period circadian mutant, *Past-time,* revealed a glycine to glutamate missense mutation in *Fbxl21*, an F-box protein gene that is a paralog of *Fbxl3* that targets the CRY proteins for degradation. While loss of function of FBXL3 leads to period lengthening, mutation of *Fbxl21* causes period shortening. FBXL21 forms an SCF E3 ligase complex that slowly degrades CRY in the cytoplasm but antagonizes the stronger E3 ligase activity of FBXL3 in the nucleus. FBXL21 plays a dual role: protecting CRY from FBXL3 degradation in the nucleus and promoting CRY degradation within the cytoplasm. Thus, the balance and cellular compartmentalization of competing E3 ligases for CRY determine circadian period of the clock in mammals.

INTRODUCTION

In mammals, the circadian clock regulates daily oscillations in behavior, physiology, and metabolism (Bass and Takahashi, 2010; Mohawk et al., 2012). The mechanism of the circadian clock is composed of an autoregulatory transcriptional network (Lowrey and Takahashi, 2011). At the core, the transcription factors CLOCK and BMAL1 drive expression of the *Period (Per) 1/2* and *Cryptochrome (Cry) 1/2* genes. PER1/2 and CRY1/2 proteins in turn interact, translocate into the nucleus, and repress the activity of CLOCK:BMAL1 to inhibit their own transcription (King et al., 1997; Gekakis et al., 1998; Lee et al., 2001). *Bmal1* expression is also regulated by a secondary feedback loop comprised of the nuclear hormone receptors REV-ERBα/β and the retinoid-related orphan receptors (Preitner et al., 2002; Cho et al., 2012).

Although the majority of the core clock components have been identified, the molecular mechanisms that define the periodicity or rate of the circadian clock are still not well understood (Zheng and Sehgal, 2012). PER and CRY are essential negative feedback elements of the clock, and the turnover rates of PER and CRY are correlated with the period length of circadian rhythms in mutant strains. For example, the *Casein kinase 1*ε *tau* mutation shortens period and destabilizes the PER proteins by hyperphosphorylation of a phosphodegron site that targets the PER proteins for ubiquitination by β-TrCP and proteasomal degradation (Gallego and Virshup, 2007; Meng et al., 2008). Conversely, mutations in the F-box protein FBXL3 lengthen period and stabilize the CRY proteins by a reduction in ubiquitination-mediated proteosomal degradation involving the SCF^{FBXL3} ubiquitin ligase complex (Busino et al., 2007; Godinho et al., 2007; Siepka et al., 2007). Recent work shows that CRY ubiquitination by SCF^{FBXL3} is triggered by AMPK-mediated phosphorylation (Lamia et al., 2009) and reversed by the deubiquitinating enzyme USP2a (Tong et al., 2012).

Genetic analysis of PER and CRY suggests that these two pathways act independently and additively to regulate circadian period in vivo (Maywood et al., 2011). Here, we report the isolation and positional cloning of a circadian mutant, *Past-time* (*Psttm*), that shortens circadian period and destabilizes CRY proteins during the circadian cycle. We describe an SCF ubiquitin ligase complex (SCF^{FBXL21}) for the CRY proteins that plays a dual role to attenuate CRY degradation by SCF^{FBXL3} in the nucleus and to promote CRY degradation in the cytoplasm.

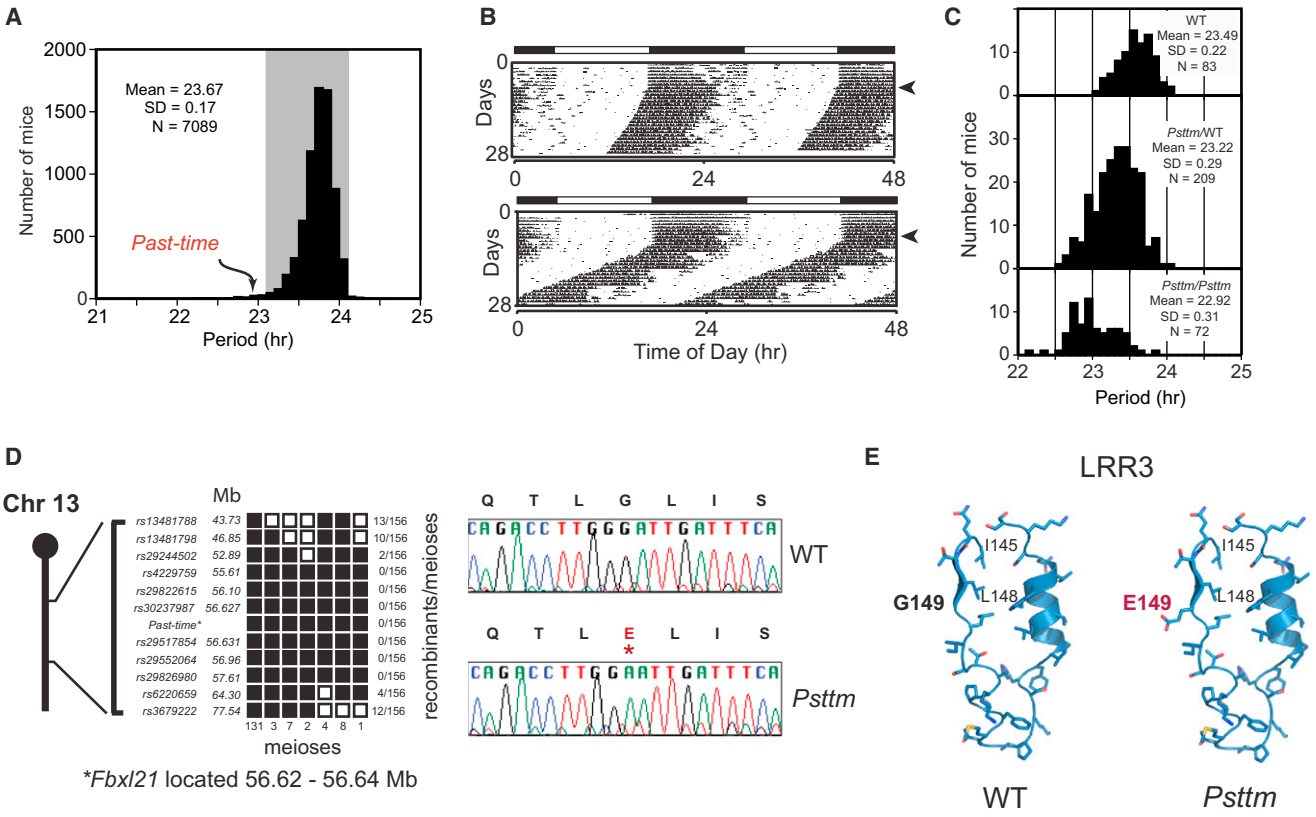

Figure 1. Positional Cloning of *Past-time* and Identification of the *Fbxl21* Mutation

(A) Histogram showing circadian period distribution of ENU mutagenized generation 3 (G3) mutant mice in a recessive screen. The shaded area represents the average period for WT C57BL/6J mice ± three standard deviations. The *Past-time* (*Psttm*) founder mouse is indicated by the arrow.

(B) Representative actogram of a WT C57BL/6J mouse (top). The actogram is double plotted where each horizontal line represents 48 hr of activity. The mice were kept on an LD12:12 cycle (represented in the bar above) for the first 7 days and then released into constant darkness for 21 days (indicated by the arrowhead on the right). Actogram of the *Past-time* founder G3 mouse (period = 22.91 hr) (bottom).

(C) Period distribution of F2 intercross mice used for genetic mapping. The three panels from top to bottom represent WT, *Psttm*/+, and *Psttm*/*Psttm* mice, respectively. ANOVA of the period was performed on the three populations of F2 mice (grouped by genotype) (DF = 2; F = 78.80; p = 3.983×10^{-29}).

(D) *Psttm* was initially mapped to a 40 Mb region on chromosome 13 between *rs13481788* and *rs367922* (left). The chromosome 13 schematic lists the markers used to map *Psttm* to a smaller genetic interval. Haplotypes of the 78 *Psttm*/*Psttm* F2 intercross progeny (156 meioses) are shown on the right. Black boxes represent C57BL/6J WT alleles, and white boxes represent C3H/HeJ alleles. The number of recombinants per total meioses is indicated to the right of the haplotype map. Sequencing of *Fbxl21* where a single-base change from G to A is indicated by the asterisk (right).

(E) Structural modeling of the FBXL21 LRR3 motif based on the Skp2 structure in WT and mutant proteins. See also Figure S1.

RESULTS

Identification of the *Past-time* mutation

In an ENU mutagenesis screen using C57BL/6J mice (Figure S1 available online), we identified a short-period mutant with a period length of 22.91 hr (Figures 1A and 1B). Crosses with C3H/HeJ mice produced animals of three phenotypic classes in the F2 generation, indicating that the mutant, named *Past-time (Psttm)*, was semidominant (Figure 1C). We initially mapped the *Psttm* mutation to a 40 Mb region on chromosome 13 (Figure 1D). Production of additional recombinants further reduced the interval to 11.4 Mb. This smaller interval contains 167 open reading frames and no known circadian clock genes. However, one candidate, *Fbxl21*, is a paralog of FBXL3 and shares 85% amino acid sequence similarity (Jin et al., 2004). FBXL3 has been shown to form a Skp1-Cul1-F-box protein (SCF) E3 ligase complex that polyubiquitinates the CRY proteins for degradation by the proteasome (Busino et al., 2007), and there is evidence suggesting that FBXL21 is a clock-controlled E3 ligase involved in ovine CRY1 degradation (Dardente et al., 2008). We sequenced all of the exons of *Fbxl21* from *Psttm* mice and found a single G-to-A change at nucleotide 787 in exon 5. This mutation cosegregated perfectly with the short-period phenotype of *Psttm*/*Psttm* mice (0/156 recombinants; Figure 1D). The point mutation converts amino acid 149 from a highly conserved glycine to a glutamic acid residue within the third leucine-rich repeat (LRR) of the protein. This G149E mutation is expected to create a charged protrusion, probably destabilizing the LRR structure (Figure 1E).

The *Psttm* Mutation Causes Period Shortening

To confirm that *Fbxl21* is the causative gene, we generated transgenic mice expressing the *Psttm* allele using the

tetracycline-transactivator (tTA) system (Hong et al., 2007). Three independent tetO::*Psttm* transgenic lines were crossed to *Scg2*::tTA mice in which the *Secretogranin-2* promoter drives tTA expression in the SCN and other brain areas to evaluate whether the *Psttm* allele affects circadian behavior. Western blot analysis using cerebellum extracts confirmed that only double-transgenic mice showed mutant protein expression (Figure S2A). To determine whether *Scg2*::tTA-driven PSTTM expression in the brain also shortens free-running period as seen in *Psttm*/+ mice (Figure S2B), we measured their circadian activity rhythms in constant darkness. Double-transgenic mice displayed short circadian periods compared with single-transgenic lines (Figures 2A and S2C). The period shortening was conditional because doxycycline (Dox) treatment, which represses tTA transgene expression, restored the period to wild-type (WT) values (Figures 2A and S2C). Removal of Dox from the drinking water after 4 weeks of treatment caused the double-transgenic mice to return to their previous, short free-running periods, confirming that inducible PSTTM expression was the cause of the short free-running periods (Figures 2B and S2D). In contrast, overexpression of WT FBXL21 under the control of the *Scg2*::tTA driver did not cause period changes in *Scg2*::tTA/tetO::*Fbxl21* #38 mice (Figures S2E, S2F, and S2G). Together, these observations show that conditional expression of the *Psttm* allele in the SCN and brain shortens circadian period in vivo, thus verifying that *Fbxl21* is the causative gene. Because transgenic expression of *Psttm* in a WT background shortens period and because the *Psttm* allele is semidominant, this suggests that *Psttm* can act as an antimorphic mutation.

To investigate the effects of *Psttm* at the cellular and molecular level, we crossed the *Psttm* mice with mice carrying the *Per2::luc* reporter (Yoo et al., 2004) and examined the circadian rhythmicity in tissue explants from WT and *Psttm* homozygous mice (Figure 2C). SCN organotypic cultures from *Psttm* mice showed robust rhythms, yet with significantly shorter periods compared with those of WT SCNs (Figure 2C, bottom right). Similarly, pituitary explants from *Psttm* mice also showed shorter periods than WT explants (Figure 2C, bottom). Thus, the primary effect of the *Psttm* mutation on the circadian clock is period shortening at both behavioral and molecular levels.

The FBXL3 I364T mutation in *Overtime* (*Ovtm*) mutant mice lengthens period by about 2.5 hr, providing evidence that CRY stability is important for setting the pace of the clock (Siepka et al., 2007). Given that both *Ovtm* and *Psttm* correspond to mutations in F-box genes related to CRY degradation, we created *Psttm*/*Psttm* *Ovtm*/*Ovtm* double-mutant mice to assess the genetic interaction of these mutant alleles (Figures 2D and 2E). While WT mice showed a mean period of 23.34 hr, *Ovtm* mice displayed a long period of 26.00 hr. In contrast, *Psttm* mice exhibited a short period of 22.77 hr. Interestingly, the *Ovtm*/*Psttm* double-homozygous mutant mice displayed a free-running period of 23.16 hr, similar to that of WT mice and different from the predicted value of 24.4 hr for an additive effect (Table S1). Thus, the *Psttm* and *Ovtm* alleles appear to act in an antagonistic rather than additive manner.

Effects of the *Psttm* Mutation on Core Clock Gene Expression

To explore the effects of the *Psttm* mutation on clock gene expression, we collected liver and cerebellum samples from WT and *Psttm* mice maintained in constant darkness and measured messenger RNA (mRNA) expression patterns. The *Psttm* mutation caused significant elevation of *Per1*, *Per2*, *Cry1*, and *Cry2* transcripts in cerebellum and a moderate elevation of clock gene transcript levels in liver (Figures 3A and S3A), perhaps due to lower *Fbxl21* expression in liver relative to cerebellum (mean Ct value of WT cerebellum and liver: 27.1 and 31.2, respectively; Figure S3D shows different levels of endogenous FBXL21 expression in various mouse tissues). Interestingly, the levels of several clock-controlled genes, including *Rev-erbα*, *Dec2*, and *Dbp*, were significantly increased in liver (Figure S3A).

Next, we examined the effects of the *Psttm* mutation on core clock protein expression in cerebellum and liver. PER1 and PER2 levels were elevated in the cerebellum of *Psttm* mice (Figure 3B), consistent with the observed increase in transcript levels. Furthermore, *Psttm* also appeared to advance the phase of the PER protein rhythm. In contrast, CRY1 protein levels were not elevated, and CRY2 levels were significantly reduced (Figure 3B). Consistent with the previously reported rhythmic *Fbxl21* mRNA accumulation (Dardente et al., 2008), we observed a circadian oscillation of FBXL21 protein in the cerebellum of WT mice. In *Psttm* mutants, FBXL21 protein levels in cerebellum were significantly reduced throughout the circadian cycle compared with WT (Figure 3B), suggesting the *Psttm* mutation impaired FBXL21 protein stability. In addition, in the liver of *Psttm* mutants, the phase of PER1/2 and CRY1/2 accumulation was advanced relative to WT (Figure 3C). FBXL21 protein accumulation was also both reduced and phase advanced in *Psttm* liver. The reduction in CRY, despite enhanced transcript levels, suggests that the *Psttm* mutation leads to the destabilization of CRY protein. In addition, because the expression of FBXL21 is rhythmic and in phase with that of CRY1/2 (Figure 3B), it is possible that FBXL21 could exert phase-dependent effects.

To determine whether the *Psttm* mutation affects CRY expression in the SCN, we used immunocytochemical quantitation of SCN sections from WT and *Psttm* mice. As shown in Figure 3D, the number of CRY1-positive nuclei was significantly reduced in SCN from *Psttm* mice at ZT0, 8, and 12 compared with WT controls (Figures 3E, S3B, and S3C). Taken together, these experiments show that the *Psttm* mutation leads to a general increase in the RNA expression of CLOCK:BMAL1 target genes, while at the same time altering the expression of CRY1 and CRY2 proteins and substantially reducing FBXL21 protein levels. The reduction in CRY, despite enhanced transcript levels, suggests that the *Psttm* mutation leads to destabilization of CRY protein.

FBXL21 Stabilizes CRY by Competing against FBXL3

The concomitant reduction of FBXL21 and CRY proteins caused by the *Psttm* mutation prompted us to investigate the biochemical interaction between CRY and FBXL21. Coimmunoprecipitation (co-IP) assays showed that among the six core clock proteins in the primary loop (CRY1/2, PER1/2, CLOCK, BMAL1), only CRY1 and CRY2 were able to interact with both FBXL21 and PSTTM (Figure S4A). All CRY1 mutants with

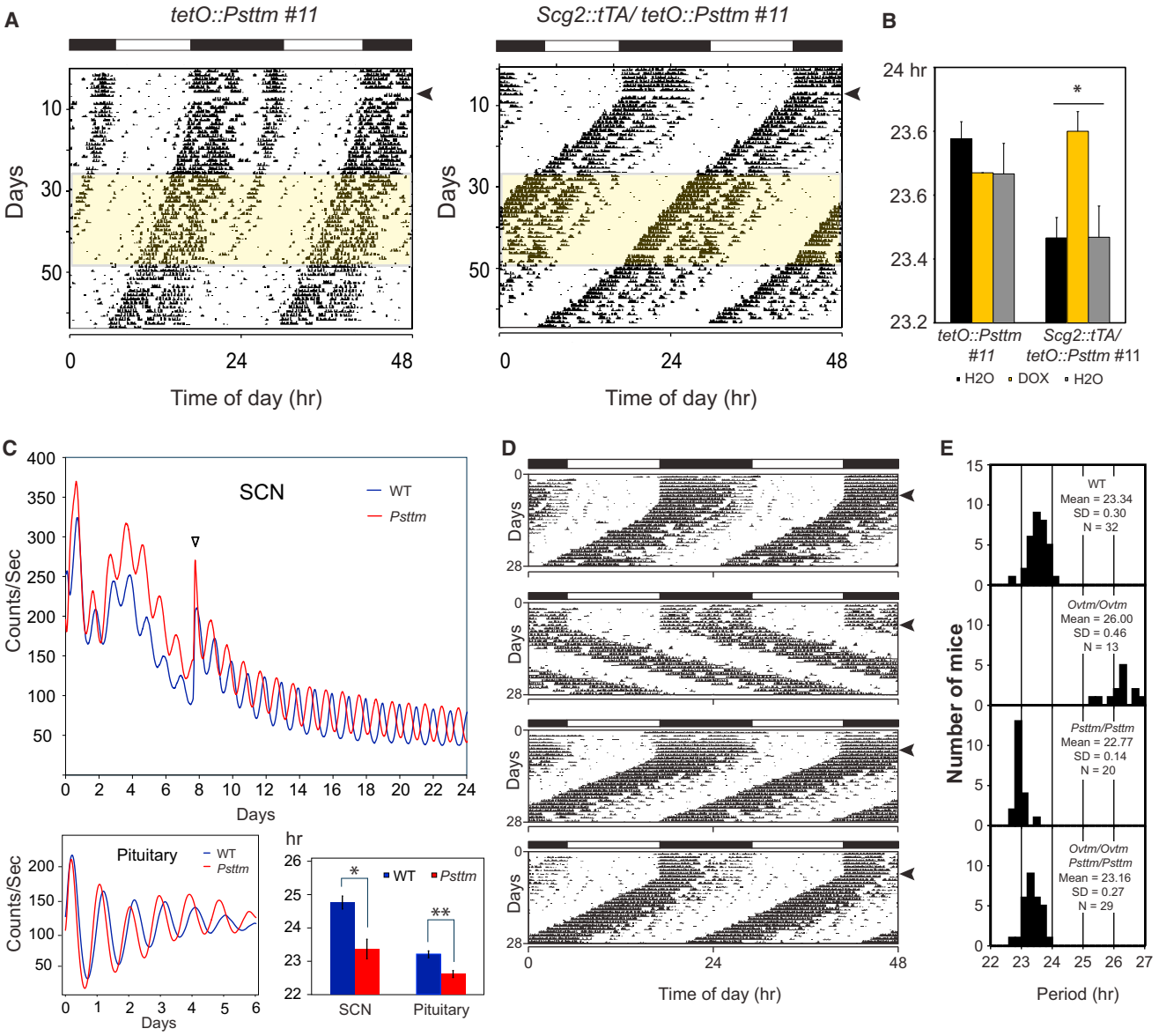

Figure 2. The *Psttm* Mutation Shortens Period and Antagonizes the Period-Lengthening Effect of the *Ovtm* Mutation in FBXL3

(A) Representative actogram of tetO::*Psttm* #11 single-transgenic mouse (left). Representative actogram of tetO::*Psttm* #11 transgenic mouse with the *Scg2::tTA* driver (right). Arrowheads indicate LD to DD transition. Doxycycline-containing (10 μg/ml) water was administered during the interval indicated by yellow shading on the actogram.

(B) Free-running periods of single and double-transgenic mice during constant darkness with water (black), Dox (yellow), and water after Dox treatment (gray). Error bars represent mean ± SEM (*tetO::Psttm #11*, n = 3; *Scg2::tTA/tetO::Psttm #11*, n = 5; *p < 0.05, Bonferroni corrected pair-wise comparison).

(C) Representative PER2::LUC bioluminescence recording of SCN and pituitary explants from WT and homozygous *Psttm* mice. Blue and red traces represent PER2 rhythm from WT and *Psttm* mice, respectively. WT SCN mean circadian period: 24.76 hr (n = 6), *Psttm* SCN mean circadian period: 23.36 hr (n = 6). t test: *p value 0.0027. WT pituitary mean circadian period: 23.2 hr, n = 6; *Psttm* pituitary mean circadian period: 22.61 hr, n = 6. t test: **p value 0.0004.

(D) Representative actograms of WT, *Ovtm/Ovtm*, *Psttm/Psttm*, and *Ovtm/Ovtm Psttm/Psttm* mice subjected to the same experimental schedule as in Figure 1B.

(E) Period distribution. The four panels from top to bottom represent WT, *Ovtm/Ovtm*, *Psstm/Psstm*, and *Ovtm/Ovtm Psttm/Psttm* mice, respectively. ANOVA of the period was performed among the genotype groups. Results: DF = 3; F = 388.507; p = 2.295×10^{-51}. See also Figure S2 and Table S1.

C-terminal domain truncation were coimmunoprecipitated with both FBXL3 and FBXL21, indicating that FBXL binds to CRY in the photolyase homology domain of CRY1 (amino acids 1–530) (Figure S4). Next we expressed the F-box proteins in NIH 3T3 cells and the cell lysates were immunoprecipitated with anti-FLAG (FBXL3, FBXL21, PSTTM) or anti-V5 (β-TrCP1) antibodies. All the F-box proteins, including PSTTM, were found to interact strongly with native CULLIN1 and SKP1 (the other components of the SCF complex), indicating that FBXL21 and PSTTM can form SCF E3 ligase complexes (Figure 4A). Only low levels of

CRY1 coimmunoprecipitated with ectopically expressed FBXL3, probably due to robust CRY1 degradation. To our surprise, FBXL21 or PSTTM coimmunoprecipitated much higher levels of CRY1 compared with FBXL3. The stable binding between CRY1 and FBXL21/PSTTM differs from the transient E3 ligase-substrate interaction commonly associated with rapid degradation seen with FBXL3-CRY. In addition, ectopically expressed PSTTM and FBXL21 both showed strong affinity toward CRY, indicating that the mutation does not significantly affect CRY binding.

To verify the interactions between FBXL21 and CRY1/2 in vivo, we assessed native protein interactions over the circadian cycle by immunoprecipitating endogenous FBXL21 proteins from WT and *Psttm* liver tissue lysates collected at different circadian times (Figures 4B and 4C). Levels of coimmunoprecipitated CRY1/2 showed a circadian rhythm correlated with their periodic accumulation (Figure 3C) in WT tissue; on the other hand, lower levels of CRY1/2 were pulled down in *Psttm* liver, presumably due to reduced FBXL21 expression (Figure 3C). Next, we compared the potential E3 ligase activity of FBXL3 with that of FBXL21 and PSTTM in CRY-degradation assays in 293A cells (Figures 4D, S4B, and S4C). In the absence of ectopic FBXL3 expression, transfected CRY1 had a half-life of 2.1 hr (Figure 4D and Figure S4C for CRY2). This rapid degradation was reversed when *Cry1* was cotransfected with *hFbxl3si* RNA, indicating that endogenous hFBXL3 regulates CRY1-HA degradation in 293A cells (Figure S4D). As expected, cotransfection of FBXL3 accelerated CRY1 degradation (0.75 hr). In contrast, cotransfection of FBXL21 significantly decelerated CRY1 degradation (12.3 hr). PSTTM also appeared to slow down CRY1 degradation, but to a lesser extent than WT FBXL21 (3.7 hr). Because endogenous hFBXL3 is present, exogenously expressed FBXL21 probably antagonizes endogenous hFBXL3 to reduce CRY1 degradation. Since FBXL21 is a less efficient E3 ligase for CRY1 than FBXL3 (Figure 4D), FBXL21 can act antagonistically with FBXL3. In addition, because PSTTM itself is less stable than WT FBXL21 (Figure 4E), PSTTM (4 hr) would be expected to antagonize SCF^{FBXL3} less efficiently than WT FBXL21 (8.6 hr). Next we introduced the corresponding *Psttm* mutation into *Fbxl3* (G143E) and measured the effect of the mutation on CRY1 degradation and FBXL3 stability (Figure S4B, bottom). The G143E mutation in *Fbxl3* did not alter protein stability or E3 ligase activity of FBXL3. Importantly, we rule out the possibility of FBXL21 or PSTTM as an E3 ligase for FBXL3: coexpression of FBXL21 or PSTTM showed no effects on FBXL3 stability independent of CRY, indicating that FBXL21 does not decelerate CRY degradation by serving as an E3 ligase for FBXL3 (Figure S4E).

To test the hypothesis that FBXL21 antagonizes FBXL3, we performed competition assays for CRY1 degradation in 293A cells (Figures 4F and S4F). In support of an antagonistic relationship, coexpression of FBXL3 and FBXL21 resulted in an intermediate CRY1 half-life (4.4 hr) relative to expression of CRY1 with either FBXL3 (1.9 hr) or FBXL21 alone (11 hr). Interestingly, in the presence of FBXL3, PSTTM was less effective in decelerating CRY1 degradation (3 hr) than FBXL21 (4.4 hr). This supports the conclusion that PSSTM is a less effective antagonist of FBXL3-mediated CRY degradation than WT FBXL21. Next, we carried out similar assays using the hypomorphic *Ovtm* mutant of *Fbxl3* to investigate whether the WT-like circadian periodicity in *Ovtm/Psttm* compound homozygous mice is associated with restored CRY degradation rate (Figures 2D and 2E). Specifically, 293A cells were cotransfected with *Cry1* and F-box pairs, *Ovtm+Fbxl21*, and *Ovtm+Psttm*. CRY1 degradation was attenuated in the presence of *OVTM* (4.9 hr; Figures 4F, bottom, and S4G), whereas PSTTM expression in place of FBXL21 restored CRY1 degradation in the presence of OVTM (1.6 hr). These changes in CRY1 degradation rate are directly correlated with the period shortening or lengthening in the *Psttm* and *Ovtm* mouse mutants (Figure 2E), suggesting that the WT periods of *Ovtm/Psttm* mice resulted from an antagonistic interaction of the two mutations on CRY degradation, in which impaired CRY degradation in OVTM was rescued in the presence of PSTTM.

To verify definitively that FBXL21 forms an SCF E3 ligase complex, we performed in vitro ubiquitination assays to examine the ubiquitination activity of SCF^{FBXL3}, SCF^{FBXL21}, and SCF^{PSTTM}. CRY1 was efficiently polyubiquitinated in the presence of SCF^{FBXL3} complex. Both FBXL21 and PSTTM were able to carry out CRY1 polyubiquitination but were less active in generating highly polyubiquitinated forms of CRY compared with FBXL3 (Figure 4G, bottom: long exposure). The observed differences in CRY ubiquitination processivity by FBXLs paralleled their effects on CRY degradation (Figure 4D). CRY1 ubiquitination by SCF^{FBXL3} was significantly reduced in the presence of SCF^{FBXL21} or SCF^{PSTTM} (Figure 4H), suggesting that attenuated CRY1 degradation in the presence of both FBXL3 and FBXL21 (Figure 4F, top) was due to direct competition between FBXL3 and FBXL21 as CRY1 E3 ligases (Figure 4H). As shown in the end-point competition assay (Figure S4H), FBXL21 and PSTTM (to a lesser extent than WT) were able to protect CRY1 from FBXL3-mediated degradation in a dose-dependent manner, suggesting direct competition between FBXL3 and FBXL21.

No activity was detected from in vitro ubiquitination assays using the UBC13/Uev1A E2 ligase required for K63 ubiquitination (Figure 4I), indicating that FBXL21 is not involved in nonproteolytic K63 ubiquitination and that CRY stabilization (Figure 4D) does not involve K63 ubiquitination by FBXL21. To confirm these results in intact cells, we performed ubiquitination assays by expressing CRY1, the F-box proteins, and ubiquitin (hUb) in 293A cells in the presence of the proteasome inhibitor MG132 (Figure 4J). Consistent with the in vitro assay results, FBXL21 and PSTTM showed significantly attenuated polyubiquitination activity relative to FBXL3.

Psttm and *Fbxl21* Knockdown Differentially Alter Nuclear and Cytoplasmic CRY Degradation

To determine the allelic nature of the *Psttm* mutant, we compared the effects of the *Psttm* mutation with loss of function of *Fbxl21* using small hairpin RNA (shRNA) knockdown of *Fbxl21* (*shFbxl21*) on mPER2::LUC rhythms in mouse embryonic fibroblasts (MEFs). *Psttm* MEFs showed advanced phases with significantly shorter periods relative to WT MEFs (Figures 5A and 5D). PSTTM was less abundant than WT FBXL21 in MEFs from the mPER2::LUC genetic background (Figure 5C, left), consistent with what we observed in the tissue samples (Figures 3B and 5C), and knockdown efficiently depleted FBXL21 protein

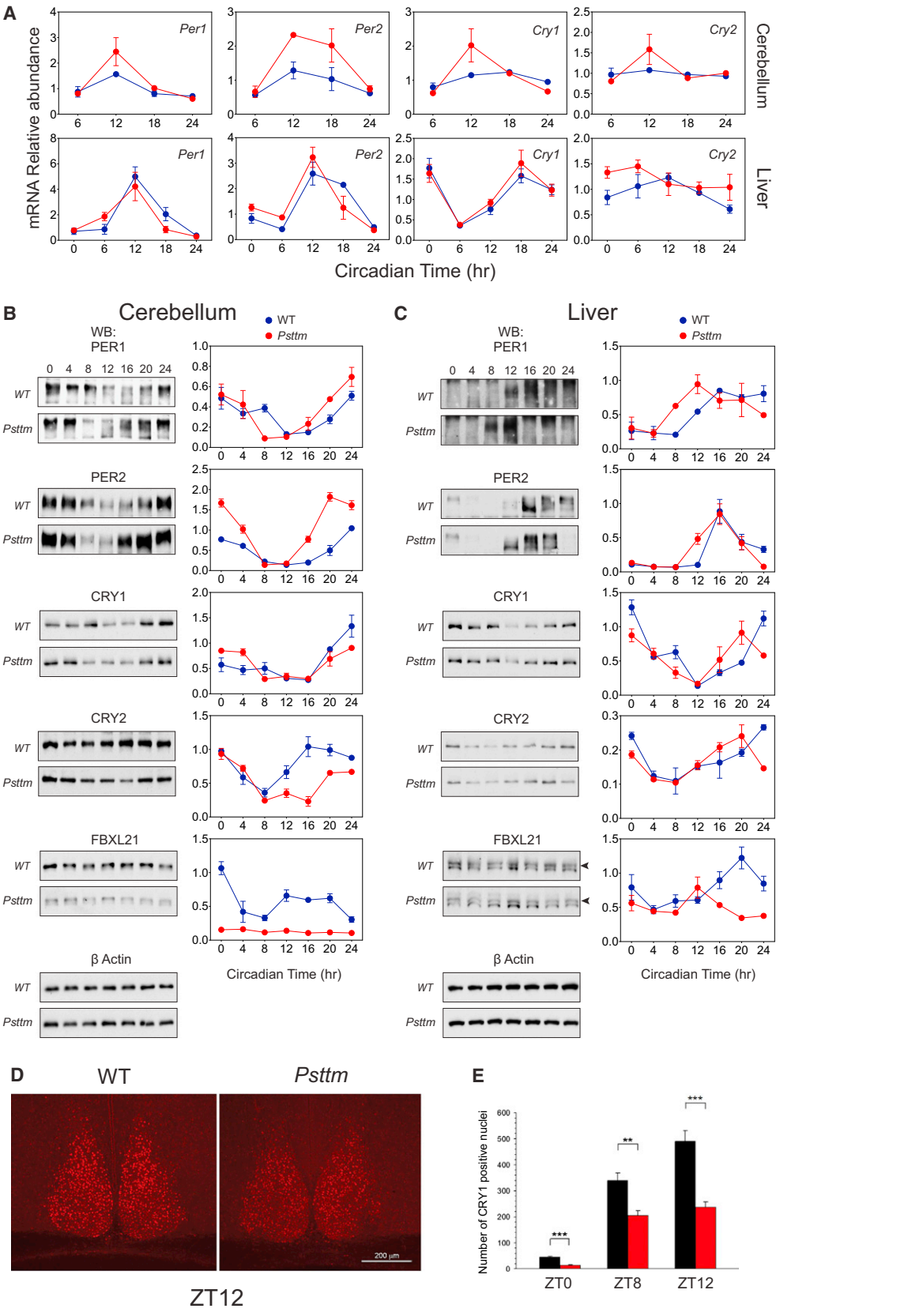

(legend on next page)

(Figure 5C, right). Importantly, *Fbxl21* knockdown also elicited phase-advance and period-shortening phenotypes compared with shRNA control MEFs (Figures 5B and 5D), indicating that the *Psttm* allele behaves as either a loss-of-function hypomorphic allele or a dominant-negative antimorphic allele. This is consistent with the in vitro ubiquitination assays that show that SCF^{Psttm} also does not show a significant gain of function in ubiquitination activity relative to SCF^{FBXL21}.

To investigate the cellular localization of *Fbxl21* and *Psttm* action on CRY abundance, we prepared nuclear and cytoplasmic fractions from samples collected over the circadian cycle and assessed CRY levels (Figures 5E, 5F, S5A, and S5B). In *Psttm* MEFs, nuclear CRY1 and CRY2 levels were significantly lower than in WT (Figures 5E, top right, and CRY2 results are shown in Figure S5A). In contrast, cytoplasmic CRY levels were significantly elevated in *Psttm* MEFs throughout the cycle (Figure 5E, bottom right, and Figure S5A). In a similar manner, *Fbxl21* knockdown reduced nuclear CRY1/2 (Figure 5F, top right, and Figure S5B) compared to GFP control yet enhanced cytoplasmic CRY1/2 levels (Figure 5F, bottom right, and Figure S5B). To understand the mechanism underlying the differential effects of FBXL21/PSTTM on nuclear and cytoplasmic CRY levels, we compared the rate of CRY degradation in nuclear and cytoplasmic fractions from WT versus *Psttm* MEFs and *sh*Control versus *shFbxl21* cell lines (Figures 5G and 5H). Both the *Psttm* mutation and *Fbxl21* knockdown accelerated nuclear CRY1/2 degradation compared with controls (Figures 5G and 5H), with opposite effects on cytoplasmic CRY degradation. Endogenous FBXL21 was detected in both nuclear and cytoplasmic fractions, and the *Psttm* mutation impaired FBXL21 accumulation in both subcellular compartments (Figure 5G). Neither the *Psttm* mutation nor depletion of endogenous FBXL21 had any effect on nuclear FBXL3 protein levels (Figure S5C). Together, these findings demonstrate that reduced levels of FBXL21 elicited opposing effects on CRY degradation in the nucleus and the cytoplasm, leading to CRY accumulation in the cytoplasm but accelerated turnover in the nucleus.

FBXL21 Forms SCF Complexes in the Cytoplasm

To determine the subcellular localization of the FBXL proteins, we generated fluorescent protein fusions of the FBXL proteins. Consistent with previous results (Cenciarelli et al., 1999), Venus-FBXL3 localized primarily to the nucleus (Figure 6A). On the other hand, Venus-FBXL21 was found in both the nucleus and the cytoplasm (Figure 6A), in accordance with MEF-fractionation experiments (Figure 5G). Venus-PSTTM showed a subcellular distribution similar to WT FBXL21, and Venus-CRY1 localized primarily in the nucleus as reported previously (Yagita et al., 2002). Next we used bimolecular fluorescence complementation (BiFC) to investigate the subcellular localization of FBXL-CRY1 complexes. Specifically, CRY1-VenC was coexpressed with the indicated VenN-FBXLs (Figure 6B), and protein interaction was measured at the Venus emission wavelength (528 nm). The CRY1-FBXL3 complex was observed primarily in the nucleus (~90%), whereas CRY1-FBXL21 or CRY1-PSTTM complexes were found in both the nucleus and cytoplasm. Furthermore, a three-way competitive BiFC assay (Kerppola, 2006), in which C-terminal Cerulean fused to CRY1 (CRY1-CerC) was allowed to interact with FBXL proteins fused with either Ven-N (VenN-FBXLs) or Cer-N (CerN-FBXLs), demonstrated that FBXL21, and to a lesser degree PSTTM, interact with CRY1 more strongly than FBXL3 (Figure 6C, bottom: quantification).

To investigate the cause of the differential effects of FBXL21 depletion on subcellular CRY degradation, we examined SCF complex formation involving FBXL3, FBXL21, and *PSTTM* by using BiFC assays. Ven-C and Ven-N were fused to the N termini of CULLIN1 or SKP1 and the N termini of FBXL3, FBXL2,1, or PSTTM, respectively. SKP1-FBXL3 and CULLIN1-FBXL3 complexes were observed primarily in the nucleus (Figure 6D). In contrast, SKP1-FBXL21, SKP1-PSTTM, CULLIN1-FBXL21, and CULLIN1-PSTTM complexes were abundant in the cytoplasm (Figures 6D and 6E). Together, these results demonstrate that FBXL21 is primarily involved in CRY degradation in the cytoplasm and that the unstable *Psttm* allele or *Fbxl21* knockdown leads to cytoplasmic CRY accumulation. On the other hand, reduced nuclear FBXL21 levels in *Psttm* or *Fbxl21* knockdown MEFs reduce the antagonistic effects of FBXL21 against FBXL3, leading to accelerated CRY degradation in the nucleus.

FBXL3 and FBXL21 Ubiquitinate Distinct Lysine Residues to Regulate CRY1 Degradation

In order to delineate the mechanism of CRY1 degradation by FBXL3 and FBXL21, we sought to identify the ubiquitination sites required for CRY1 degradation by these two F-box proteins. Initially we chose 18 conserved lysine residues in CRY1 and CRY2 and converted them individually to arginine to test for loss of function. No single lysine residue was found to be critically required for CRY1 degradation in the presence of FBXL3 or FBXL21. Of these individual CRY1 mutants, K107R and K228R showed mildly impaired degradation by FBXL3. Although K159R and K308R are not conserved between CRY1 and CRY2, these sites showed similarity to the consensus sequence of ubiquitination sites (Catic et al., 2004), and the K159R/K308R

Figure 3. *Psttm* Alters Circadian Clock Gene Expression in Mice

(A) Real-time RT-PCR analysis of clock gene expression in WT and *Psttm* mice. Blue and red circles represent WT and *Psttm* mice, respectively. Error bars represent SEM for each time point from four independent replicates. Two-way ANOVA shows significant statistical differences between WT and *Psttm* mutants for *Per1* ($p < 0.001$) and *Per2* ($p < 0.0001$). *Cry1* expression shows statistically significant difference at CT12 ($p < 0.01$) between WT and *Psttm* mice.

(B and C) Clock protein oscillation in cerebellum (B) and liver (C). Western blotting was performed using total protein extracts with the indicated antibodies. Representative blots from three independent experiments are shown and quantification is shown to the right of each representative blot. Blue and red circles represent values from WT and *Psttm* mice. Error bars represent SEM ($n = 3$). In (B), two-way ANOVA shows significant differences between WT and *Psttm* for PER2 ($p < 0.0001$), CRY2 ($p < 0.0001$), and FBXL21 ($p < 0.0001$). In (C), two-way ANOVA shows significant differences between WT and *Psttm* for FBXL21 ($p < 0.0001$).

(D) Immunohistochemical staining of CRY1 in SCN sections from WT and *Psttm* mice. Representative images from ZT12 are shown.

(E) Number of CRY1-positive nuclei in the SCN sections collected from WT and *Psttm* mice at ZT0, 8, and 12. Student's t test shows statistically significant difference between WT and *Psttm* mice at ZT0 and ZT12 (***$p < 0.001$) and ZT8 (*$p < 0.01$). Error bars represent mean ± SEM. See also Figure S3.

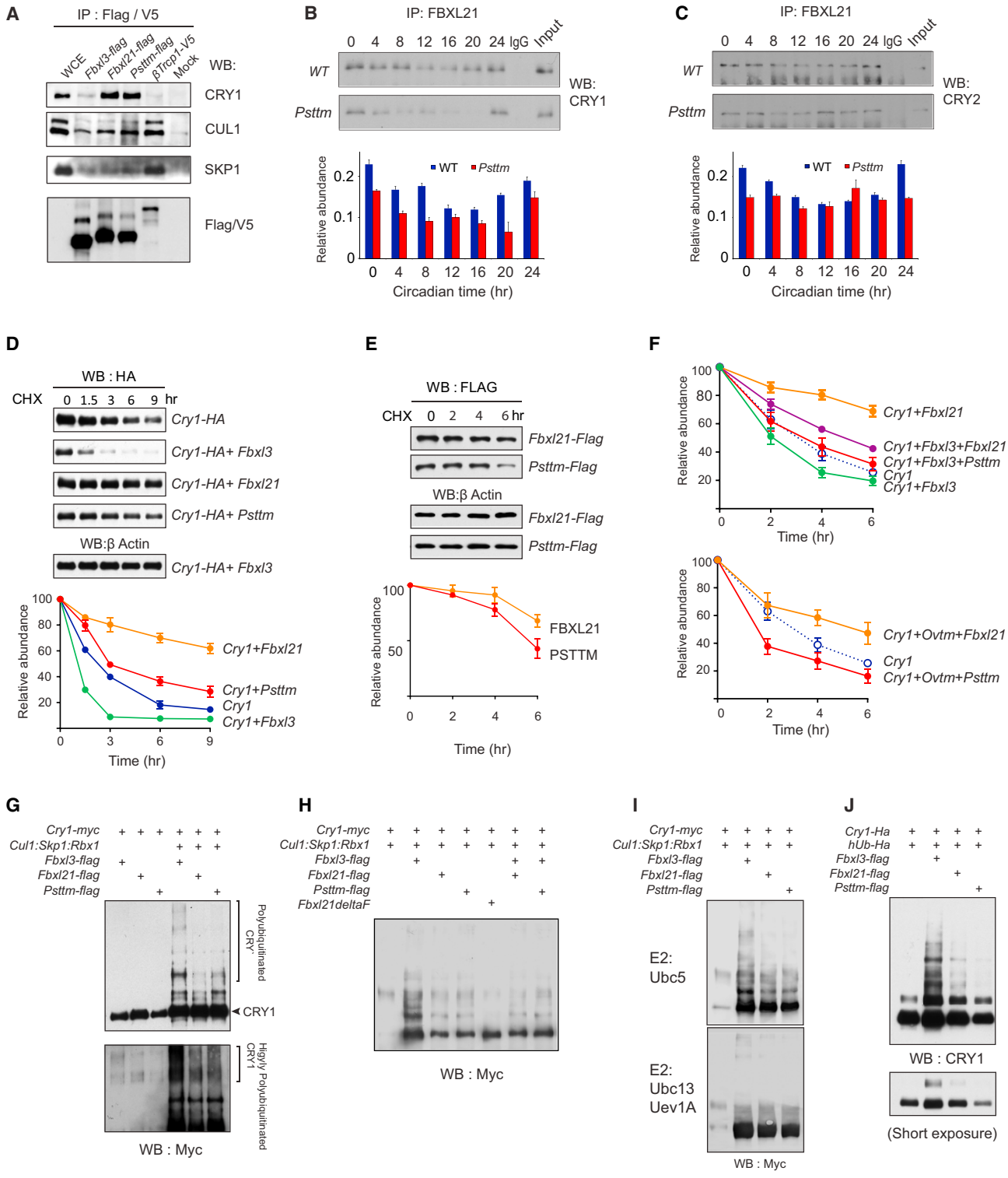

Figure 4. FBXL21 Forms an SCF E3 Ligase Complex that Slowly Ubiquitinates CRY1 and Antagonizes the Activity of SCF^{FBXL3}

(A) Interaction of FBXL proteins with CULLIN1 and SKP1. NIH 3T3 cells were transfected with *Flag-Fbxl3*, *Flag-Fbxl21*, *Flag-Psttm*, and *V5-βTrcp1* expression constructs. Coimmunoprecipitated proteins were analyzed by western blotting with anti-CRY1, anti-CUL1, and anti-SKP1 antibodies. Representative blots from three experiments are shown.

(B and C) FBXL21 interacts with CRY1 (B) and CRY2 (C) in native extracts in a circadian manner. Liver extracts from CT0 to CT24 were immunoprecipitated (IP) with an FBXL21 antibody, and western blotting was performed with CRY1 and CRY2 antibodies. Bottom: quantification of coimmunoprecipitated CRY1 and

(legend continued on next page)

double mutation caused mild CRY1 stabilization. These initial experiments suggested that multiple lysine residues probably play redundant roles for CRY1 degradation. Thus we also employed a reverse approach, starting from a degradation-resistant mutant CRY1, in which all 31 lysine residues were mutated to arginine (CRY1:R). To determine whether CRY1:R retained protein-protein interactions comparable to WT CRY1, we first performed coimmunoprecipitation with FBXL3 and FBXL21. As shown in Figure 7A, cotransfected FBXL3 immunoprecipitated low levels of WT CRY1-HA in the absence of MG132, probably due to active CRY1 degradation. In contrast, CRY1:R efficiently coimmunoprecipitated with FBXL3; concordantly, the in vivo ubiquitination assay showed that this mutant was resistant to FBXL3-mediated ubiquitination (Figure 7A, right). Furthermore, co-IP with PER2 confirmed that CRY1:R could also interact with PER2 (Figure 7A, bottom). In addition, reporter assays using a *mPer2* promoter construct, pGL6 (Yoo et al., 2005), demonstrated that CRY1:R was able to repress CLOCK:BMAL1 transactivation of E-box-dependent transcription to a similar extent as WT CRY1 (Figure 7B). Thus, mutation of all 31 lysine residues in CRY1 renders it resistant to ubiquitination and degradation but surprisingly functional in protein interaction and transcriptional repression assays.

We then used site-directed mutagenesis to generate 31 individual lysine revertants from Cry1:R to test for gain of function. Individual clones were transfected, either alone or cotransfected with *Fbxl3* or *Fbxl21* expression constructs, into 293A cells, and degradation was monitored as above (Figures S6 and S7). An initial gain-of-function screen revealed six putative FBXL3 target residues: K68, K189, K277, K456, K585, and K599 (Figure 7F). Combining the four aforementioned residues from the initial loss-of-function screen, we generated a panel of ten candidate lysine revertants from Cry1:R, and degradation of these mutants in the presence of FBXL3 and FBXL21 is shown in Figure 7C. We further divided the candidate lysine sites into two groups according to their proximity to known CRY1 phosphorylation sites (Lamia et al., 2009). Cry1:R-6Ks is a six-lysine revertant where the lysine residues are located close to phosphorylation sites, whereas Cry1:R-4Ks contains four lysine residues without nearby phosphorylation sites. As shown in Figure 7C, CRY1-10K regained FBXL3-mediated degradation, displaying a degradation rate similar to that of WT CRY1 (Figure 7D). Interestingly, Cry1:R-6Ks displayed a similar degradation rate as Cry1:R-10K, whereas Cry1:R-4Ks was much more stable. Multiple CRY1 mutants with fewer lysine combinations were more resistant to FBXL3-mediated degradation than Cry1:R-6Ks. Thus, there are multiple and redundant potential CRY1 degron sites for FBXL3. FBXL21 expression showed no effects on the half-life of these revertant CRYs, indicating that FBXL3 and FBXL21 do not share ubiquitination sites. Remarkably, similar site mapping for FBXL21 revealed a single candidate residue, K11 (Figure 7E), as the preferred ubiquitination site for FBXL21 (Figure S7). Figure 7F shows a summary of results from degron screening. As indicated by the green boxes, FBXL3 appears to utilize multiple lysine residues for CRY1 degradation. In contrast, FBXL21 showed a highly restricted preference for CRY1 ubiquitination, perhaps explaining why FBXL21 displayed low activity in CRY degradation.

DISCUSSION

CRY proteins are the major negative regulators in the core loop of the mammalian circadian clock. Multiple lines of evidence suggest a key role for CRY1 in regulating circadian period length. For example, impaired CRY degradation in the *Ovtm* mutant caused significant repression of CLOCK:BMAL1-driven transcription and lengthening of period (Siepka et al., 2007). In addition, it has been known for more than a decade that the *Cry1* knockout mouse has a short period while the *Cry2* knockout has a long period (van der Horst et al., 1999; Vitaterna et al., 1999). Recent work has provided insight into the transcriptional regulation of *Cry1* (Ukai-Tadenuma et al., 2011), as well as

CRY2 amounts. Error bars represent mean ± range (n = 2 experiments). Two-way ANOVA shows statistically significant differences between WT and *Psttm* for the amount of CRY1 coprecipitated with FBXL21 throughout the circadian cycle ($p < 0.0001$).

(D) Differential effects of FBXL21 and PSTTM on CRY1 stability. 293A cells were cotransfected with indicated constructs. Thirty-two hours after transfection, cells were treated with 20 μg/ml cycloheximide and incubated for the indicated time before harvest. Western blotting was performed to monitor CRY1 levels using an anti-HA antibody. Bottom: quantification of the effects of FBXL3, FBXL21, and PSTTM on CRY1 stability. Error bars represent mean ± SEM (n = 3 experiments). Half-life was determined by using nonlinear, one-phase exponential decay analysis (half-life parameter, K, is significantly different in all four conditions: $p < 0.0001$).

(E) The *Psttm* mutation destabilizes FBXL21. 293A cells were transfected with *Fbxl21-Flag* or *Psttm-Flag* constructs. Cycloheximide treatment was performed as in (D). Error bars represent mean ± SEM (n = 3 experiments). Half-life parameter, K, is significantly different: $p = 0.0436$.

(F) Competition between FBXL3 and FBXL21/PSTTM modulates CRY1 degradation. Cycloheximide treatment and CRY1 western blotting were performed as in (D). Half-life parameter, K, is significantly different: $p < 0.0001$. Error bars represent mean ± SEM (n = 3 experiments) (Figure S4F). Bottom: competition between *Ovtm* and *Fbxl21/Psttm* in CRY1 degradation. Cycloheximide treatment and CRY1 western blotting were performed as in (D). Half-life parameter, K, is significantly different: $p < 0.0001$. Error bars represent mean ± SEM (n = 3 experiments) (Figure S4G).

(G) In vitro ubiquitination assay. Sf9 cells were infected with the indicated baculovirus constructs. Samples were analyzed by western blotting with an anti-Myc antibody. Top shows a short exposure image, and the bracket to the right marks polyubiquitinated CRY1. Bottom shows a long-exposure image, and the bracket to the right marks highly polyubiquitinated CRY1. Results are representative of more than three replicates.

(H) In vitro ubiquitination was performed as indicated in (G). Sf9 cells were infected with the indicated baculovirus. Coinfection of *Fbxl* baculovirus (*Fbxl3+Fbxl21*, *Fbxl3+Psttm*) attenuated the E3 ligase activity of FBXL3. Results are representative of three replicates.

(I) FBXL3/FBXL21-mediated CRY1 ubiquitination requires Ubc5 as an E2 ligase. Top: Ubc5-mediated robust ubiquitination by FBXL3-SCF complexes and multi ubiquitination by FBXL21/PSTTM SCF complex. Bottom: lack of CRY1 ubiquitination in the presence of Ubc13/Uev1A as the E2 ligase. Results are representative of three replicates.

(J) 293A cells were cotransfected with *Cry1-HA*, ubiquitin (*hUb-HA*) and the indicated F-box constructs. Cells were treated with MG132 (10 μg/ml) 6 hr before harvest. Whole-cell lysates were analyzed by western blotting with an anti-CRY1 antibody. Results are representative of three replicates. See also Figure S4.

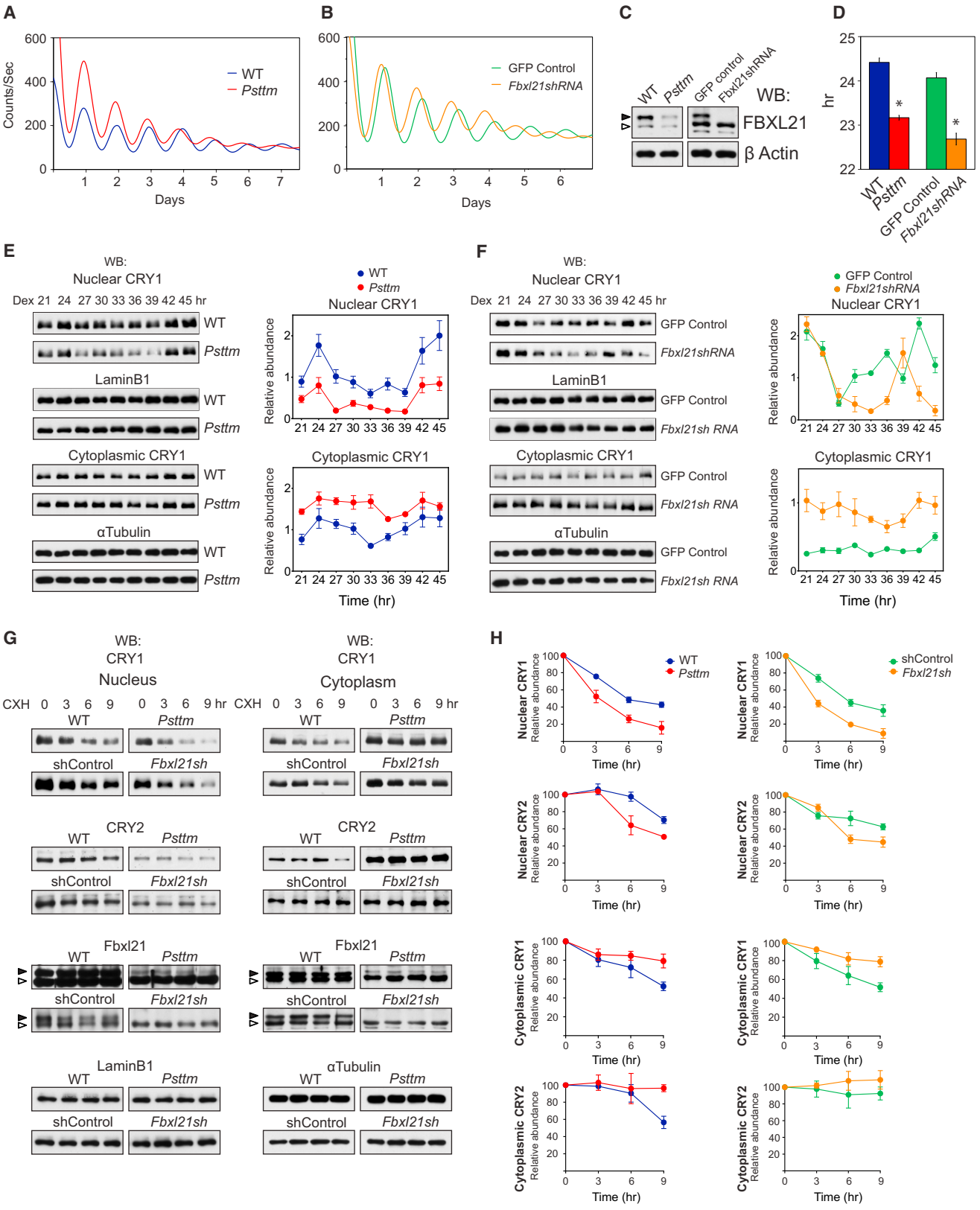

(legend on next page)

identification of a domain in CRY1 that is required for the maintenance of circadian rhythms (Khan et al., 2012). Despite these advances, how CRY stability and turnover are regulated and how CRY stability is related to circadian period remains to be understood. Here, we identified a short-period mutant, *Past-time*, that is caused by a G149E missense mutation in FBXL21, a leucine-rich repeat F-box protein that is a paralog of FBXL3, an E3 ligase responsible for CRY protein turnover. Contrary to working in an additive manner with FBXL3, as might be expected of a paralog, we find instead that FBXL21 antagonizes FBXL3 in genetic interaction experiments in vivo, in cellular assays of CRY stability, and in biochemical ubiquitination assays of the reconstituted SCF E3 ligase complex in vitro. Taken together, these experiments show definitively that FBXL21 interacts with FBXL3 to counterbalance the E3 ligase activity of SCF^{FBXL3} on CRY1 and CRY2 to stabilize them, consistent with the accompanying paper by Hirano et al. (2013) in this issue of *Cell*. The mechanism by which FBXL21 protects CRY is unusual for an E3 ligase. Although FBXL21 has intrinsic E3 ligase activity as an SCF^{FBXL21} complex, it is much less efficient than SCF^{FBXL3} in polyubiquination of CRY but has greater affinity for CRY, as measured in vivo with competitive BiFC assays. Thus, FBXL21 interacts more strongly with CRY than FBXL3 and, as a consequence, can protect CRY from SCF^{FBXL3} activity.

From subcellular localization experiments, we found that the distributions of FBXL21 and FBXL3 are strikingly different: FBXL3 is found almost exclusively in the nucleus, while FBXL21 is distributed in both nucleus and cytoplasm. The distribution of the FBXL proteins was also mirrored by their interactions with SKP1 and CULLIN1 so that SCF^{FBXL3} complexes were primarily nuclear whereas SCF^{FBXL21} complexes were mainly cytoplasmic. Based on the subcellular distribution of FBXL21 and FBXL3, we infer that their interactions probably occur in the nucleus. First, in the *Psttm* mutant and in *Fbxl21* shRNA knockdown experiments, the levels of CRY1 and CRY2 are lower in the nucleus under conditions where either PSTTM is destabilized or FBXL21 is depleted. Second, the half-lives of CRY1 and CRY2 are shorter in the nucleus. These results are consistent with a model in which FBXL3 is a primary E3 ligase for CRY in the nucleus and FBXL21 protects CRY from rapid polyubiquitination by SCF^{FBXL3} by competing with FBXL3. In the absence of FBXL21, CRY would then be more susceptible to SCF^{FBXL3} and would turn over faster to shorten circadian periodicity. Interestingly, FBXL21 does have modest E3 ligase activity so that the SCF^{FBXL21} complex is not inactive, but is significantly less active than that of SCF^{FBXL3}. Thus, the antagonistic activity of FBXL21 is most likely to occur mechanistically in a manner analogous to a "partial agonist" in classical pharmacology where a partial agonist (FBXL21) can act as a competitive antagonist in the presence of a full agonist (FBXL3). The evidence that FBXL21 and the SCF^{FBXL21} complex display "partial agonist" activity can be seen in the cytoplasmic effects of loss-of-function mutations of either PSTTM or FBXL21 knockdown where the levels of CRY1 and CRY2 are elevated significantly. Because there is essentially no FBXL3 in the cytoplasm, the SCF^{FBXL21} complex is the primary E3 ligase for CRY in the cytoplasm.

Here, identification of the E3 ligase FBXL21 reveals a mechanism involving two paralogous E3 ligases regulating nuclear CRY protein turnover in an antagonistic manner. Previous work has provided examples of multiple E3 ligases coregulating a single target in the cell cycle (Reed, 2003; Pines, 2011). For example, turnover of the key cell-cycle regulator MYC has been shown to be regulated by distinct E3 ligases, such as SCF^{FBW7}, SCF^{SKP2}, and $SCF^{\beta TrCP}$, at various cell-cycle phases (Popov et al., 2010). Additionally, p53 protein degradation also appears to involve several E3 ligases including Mdm2, ARF-BP1, PIRH2, COP1, and WWP1 (Dai and Gu, 2010). Importantly, $SCF^{\beta TrCP}$ and WWP1 have been shown to confer substrate-protective functions for MYC and p53, respectively. However, unlike any of these precedents for interacting E3 ligases in the cell cycle, where distinct E3 ligases from different protein families interact, the antagonism of two paralogous SCF complexes (SCF^{FBXL3} and SCF^{FBXL21}) in the same pathway is unique.

Figure 5. The *Psttm* Mutation Is Mimicked by *Fbxl21* Knockdown and Promotes Accelerated CRY1 Degradation in the Nucleus and Stabilization in the Cytoplasm

(A) *Psttm* shortens circadian period in MEFs. Representative PER2::LUC bioluminescence recording from WT and *Psttm* MEFs.

(B) *Fbxl21* knockdown shortens circadian period in MEFs. Representative PER2::LUC bioluminescence recording from Lenti-GFP-infected and Lenti-*Fbxl21sh*-infected PER2::LUC MEFs.

(C) Western blotting of WT, *Psttm*, Lenti-GFP, and Lenti-*Fbxl21sh* cell lysates showing that FBXL21 is low in *Psttm* MEFs and depleted in *Fbxl21* knockdown MEFs. Filled and open arrows indicate FBXL21 and a nonspecific band, respectively.

(D) Average period values of the experimental groups in (A) and (B). Statistically significant difference in period was detected between WT (24.4 hr, n = 6) and *Psttm* (23.1 hr, n = 6) MEFs (t test: *p < 0.001,). Likewise, statistically significant difference in period was detected between Lenti-GFP (24.06 hr, n = 6) and Lenti-*Fbxl21si* (22.68 hr, n = 6) MEFs (t test: *p < 0.001). Error bars represent mean ± SEM.

(E) The *Psttm* mutation decreases nuclear CRY1 levels and oscillation amplitude. Western blotting for CRY1 was performed using nuclear and cytosolic fractions. Right: quantification from triplicates including examples shown here. CRY1 levels from *Psttm* nuclei were significantly reduced (top, two-way ANOVA, $p < 0.001$) relative to CRY1 from WT nuclei. In contrast, cytoplasmic CRY1 levels from *Psttm* were significantly elevated throughout the circadian cycle (bottom, two-way ANOVA, $p < 0.001$). Error bars represent mean ± SEM (n = 3).

(F) *Fbxl21* depletion reveals that *Psttm* behaves as either a loss-of-function or a dominant-negative mutation relative to WT *Fbxl21*. Lenti-GFP- and Lenti-*Fbxl21sh*-infected mPER2::LUC MEFs were treated the same as in (E). Right: quantification from triplicates including example shown in (F). Error bars represent mean ± SEM (n = 3). CRY1 levels in Lenti-*Fbxl21sh* nuclei were significantly reduced ($p < 0.001$), whereas cytoplasmic CRY1 levels were significantly increased throughout the circadian cycle ($p < 0.001$).

(G) Accelerated nuclear CRY degradation and decelerated cytoplasmic CRY degradation in *Psttm* and *Fbxl21* knockdown MEFs. Western blotting was performed using anti-CRY1, -CRY2, and -FBXL21 antibodies for nuclear and cytoplasmic fractions. Representative blots from three experiments are shown.

(H) Quantification of nuclear and cytoplasmic CRY1 and CRY2 degradation in *Psttm* and *Fbxl21sh* MEFs from triplicate experiments including the representative blots shown in (G). Error bars represent mean ± SEM (n = 3). See also Figure S5.

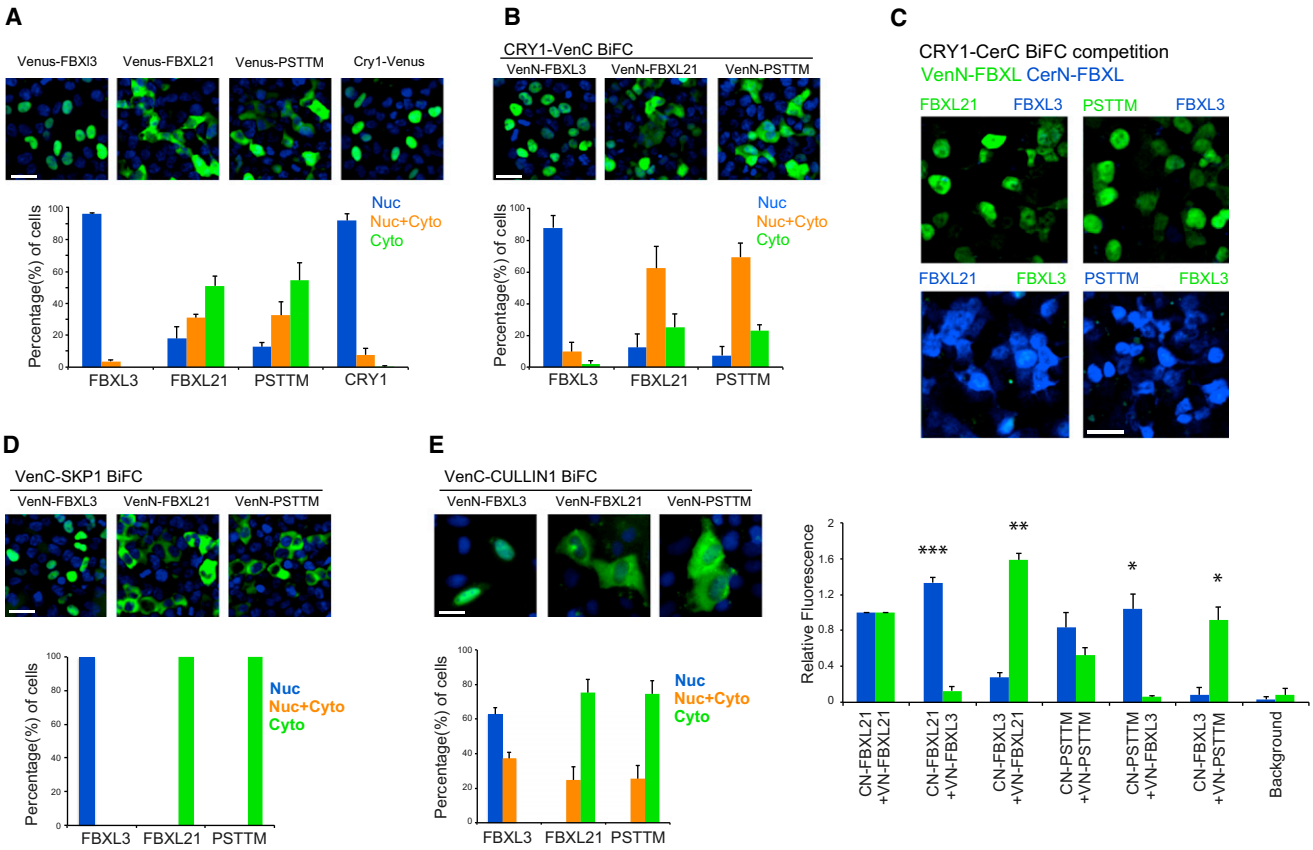

Figure 6. Differential Localization of FBXL3 and FBXL21 SCF Complexes in the Nucleus and Cytoplasm

(A) Differential subcellular localization of FBXL3, FBXL21, and PSTTM. Full-length Venus-tagged FBXL3, FBXL21, PSTTM, and CRY1 were expressed in 293A cells, and percentages of cells with fluorescence signals in nuclei only, cytoplasm only, or both were measured. Whereas FBXL3 (96%) and CRY1 (92%) were predominantly localized to the nucleus, FBXL21 and PSTTM were found in the both nucleus and cytoplasm with 51% and 54% of cells in the cytoplasm, respectively. Smaller percentages of cells showed nuclei-only localization (FBXL21: 18%, PSTTM: 12%) or both (FBXL21: 30%, PSTTM: 36%). Green: Venus; blue: DAPI. Bar graphs show the mean ± SD of three replicate experiments. Two-way ANOVA shows the localization is significantly different, $p < 0.0001$.

(B) Differential subcellular localization of CRY-FBXL complexes. VenN-tagged FBXL3, FBXL21, and PSTTM formed BiFC complexes with VenC-tagged CRY1 in 293A cells. FBXL3-CRY1 complexes were primarily localized to the nuclei (88%); however, FBXL21-CRY1 (62%) and PSTTM-CRY1 (70%) were distributed in both nuclei and cytoplasm. Green: Venus; blue: DAPI. Bar graphs show the mean ± SD of three replicate experiments. Two-way ANOVA shows the localization is significantly different, $p < 0.0001$.

(C) Reciprocal two-color, three-way BiFC competition assays in 293A cells using CRY1-CerC complementation with CerN-FBXL3 + VenN-FBXL21 or VenN-PSTTM (top) and with VenN-FBXL3 + CerN-FBXL21 or CerN-PSTTM (bottom). FBXL21, and to a lesser degree PSTTM, interact with CRY1 more strongly than FBXL3 (bottom: quantification). Green: Venus; blue: Cerulean. Bar graphs show the mean ± SEM of three replicate experiments; *$p < 0.01$, **$p < 0.001$, ***$p < 0.0001$.

(D) FBXL3 and SKP1 form complexes predominantly in the nuclei of 293A cells, whereas FBXL21 and PSTTM interact with SKP1 in the cytoplasm. Bar graphs show the mean ± SD of three replicate experiments. Two-way ANOVA shows the localization is significantly different, $p < 0.0001$.

(E) FBXL3 and CULLIN1 form complexes mainly in the nuclei of U2OS cells (63%), whereas FBXL21 (75%) and FBXL21^{Psttm} (74%) bind to CULLIN1 mainly in the cytoplasm. All scale bars represent 30 μm. Bar graphs show the mean ± SD of three replicate experiments. Two-way ANOVA shows the localization is significantly different, $p < 0.0001$.

Translocation between the cytoplasm and the nucleus is a key step in the circadian cycles of both the positive factors (CLOCK: BMAL1) (Kondratov et al., 2003) and the negative factors (CRY/PER) of the core circadian loop. The subcellular distribution and relative E3 ligase activity of FBXL3 and FBXL21 create a regulatory mode for CRY stability in the cell, analogous to that seen in the cell cycle where the ubiquitin-proteasomal system can degrade a specific protein at a specific time and in a specific place (Pines and Lindon, 2005). Thus, the discovery of FBXL21 and the differential regulation of CRY stability in the nucleus and cytoplasm reveal a prominent and sensitive role of the nucleus in regulating circadian period.

EXPERIMENTAL PROCEDURES

ENU Mutagenesis Screen and Characterization of *Psttm* Phenotypes

ENU mutagenesis screen for circadian mutants, genetic mapping, and positional cloning was performed as described previously (Siepka et al., 2007). Confirmation of the mutant gene by transgenic expression of the mutant *Psttm* allele, *Per2*::luciferase bioluminescence recording, genetic interaction

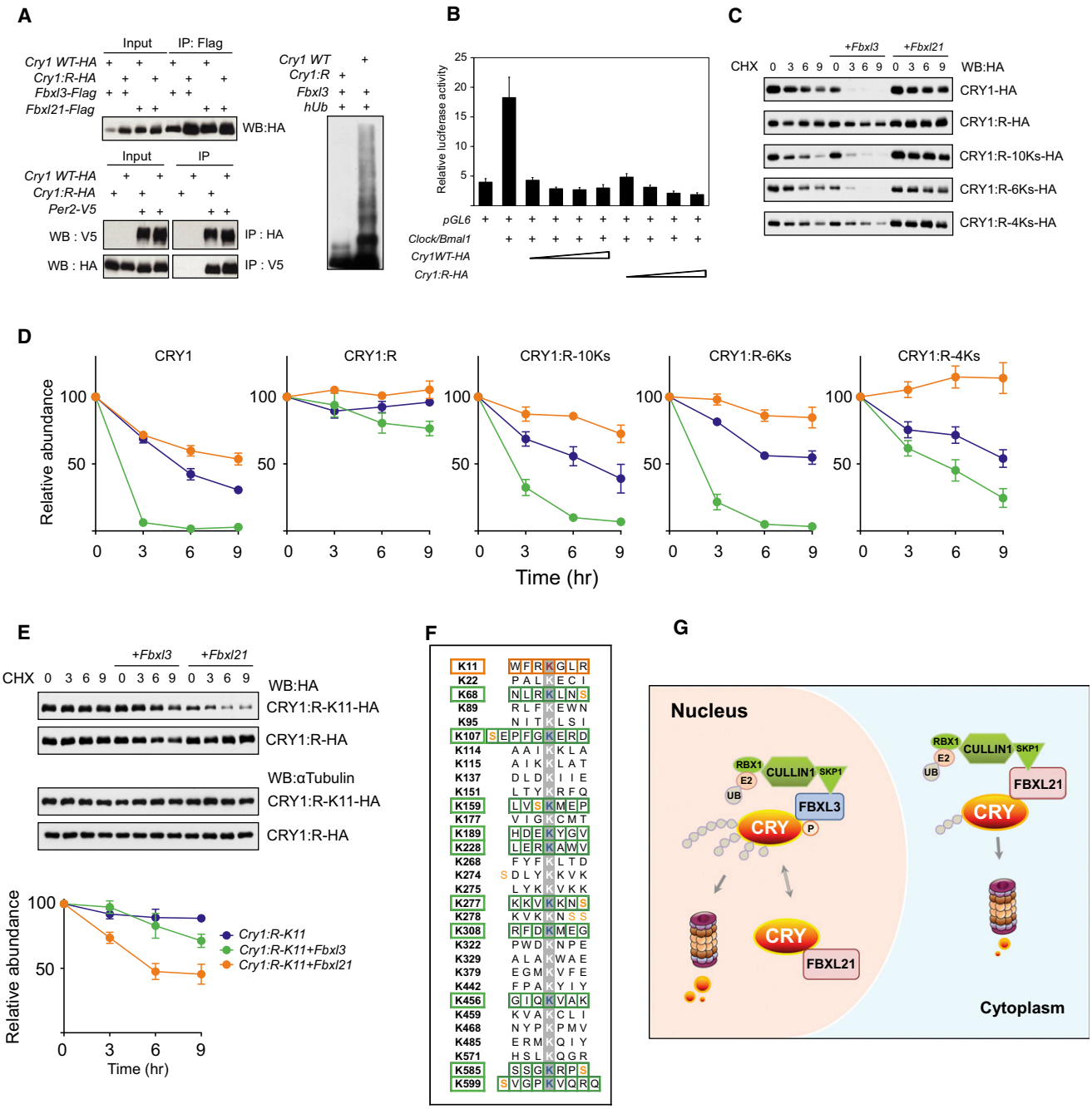

Figure 7. Identification of CRY1 Ubiquitination Sites for FBXL3 and FBXL21

(A) Left: CRY1:R coimmunoprecipited with FBXL3, FBXL21, and PER2. Top: coimmunoprecipitation of CRY1WT and CRY1:R with FBXL proteins. Bottom: reciprocal co-IP of WT and CRY1:R with PER2. WT or *Cry1*:R expression constructs were transfected into 293A cells as indicated (+). Right: 293A cells were cotransfected with indicated constructs. Whole-cell lysates were analyzed by western blotting with an anti-CRY1 antibody. Representative blots from three experiments are shown.

(B) CRY1:R repressed CLOCK:BMAL1-mediated transcriptional activation of the *Per2* promoter. pGL6 was transfected into 293A cells with the indicated constructs (+). Luciferase reporter assay showed similar repression efficiency for CRY1:R and CRY1 WT. Results are mean ± SEM for three experiments in duplicate.

(C) Representative western blots of HA-tagged CRY1 (WT, R, R-10Ks, R-6Ks, or R-4Ks). The *Cry1* construct was transfected alone or with *Fbxl3* or *Fbxl21* into 293A cells. Cells were treated with CHX (100 μg/ml) and collected after 0, 3, 6, or 9 hr.

(D) Quantification of CRY1 and CRY1 mutant degradation by *Fbxl3* or *Fbxl21* from two experiments in duplicate (n = 4 western blots; representative blots shown in C). Data represent mean ± SEM for expression of *Cry1* alone (blue), *Cry1* + *Fbxl3* (green), or *Cry1* + *Fbxl21* (orange). Half-life was determined by nonlinear, one-phase exponential decay analysis. CRY1 half-life: alone, 5 hr; + *Fbxl3*, 0.7 hr; and + *Fbxl21*, 9 hr. CRY1:R half-life: alone, > 24 hr; + *Fbxl3*, 21 hr;

(legend continued on next page)

experiments, and circadian gene expression analysis are described in the Extended Experimental Procedures. All animal care and experimental treatments were in accordance with Northwestern University and UT Southwestern Medical Center guidelines for animal care and use.

CRY Degradation, In Vitro Ubiquitination Assays, and Subcellular Localization

The interaction of FBXL proteins with CRY1/2, and the effects of FBXL proteins on CRY degradation rates were performed as described (Siepka et al., 2007). CRY1-containing SCF complexes were purified from Sf9 cells (Invitrogen) using M2 FLAG agarose. Ubiquitination assays for CRY1 were carried out as described previously (Xu et al., 2009). CRY interaction and degradation assays were also performed on nuclear and cytoplasmic fractions. BiFC assays were performed as described (Kerppola, 2006).

SUPPLEMENTAL INFORMATION

Supplemental Information includes Extended Experimental Procedures, seven figures, and two tables and can be found with this article online at http://dx.doi.org/10.1016/j.cell.2013.01.055.

ACKNOWLEDGMENTS

We thank Choogon Lee for generously providing the anti-PER1 antibody, Homin Kim for LRR3 modeling, Junghea Park, Weimin Song, and Yoga Chelliah for excellent technical support, and Yi Liu for editorial comments on the paper. Research was supported by NIH grants (U01 MH61915, P50 MH074924, and R01 MH078024 to J.S.T.; P50 MH074924 and R01 GM090247 to C.B.G.; R01 GM63692 to Z.J.C.; F32 DA024556 to V.K.), the Howard Hughes Medical Institute (J.S.T. and Z.J.C.), the Welch Foundation (I-1389 to Z.J.C.), and the American Heart Association (11SDG7600045 to Z.C.). J.S.T. and Z.J.C. are Investigators, J.A.M. is an Associate, I.K. is a Laboratory Manager, and S.-H.Y., S.M.S., H.-K.H., and V.K. were Associates at the Howard Hughes Medical Institute.

Received: August 14, 2012
Revised: November 10, 2012
Accepted: January 30, 2013
Published: February 28, 2013

REFERENCES

Bass, J., and Takahashi, J.S. (2010). Circadian integration of metabolism and energetics. Science *330*, 1349–1354.

Busino, L., Bassermann, F., Maiolica, A., Lee, C., Nolan, P.M., Godinho, S.I., Draetta, G.F., and Pagano, M. (2007). SCFFbxl3 controls the oscillation of the circadian clock by directing the degradation of cryptochrome proteins. Science *316*, 900–904.

Catic, A., Collins, C., Church, G.M., and Ploegh, H.L. (2004). Preferred in vivo ubiquitination sites. Bioinformatics *20*, 3302–3307.

Cenciarelli, C., Chiaur, D.S., Guardavaccaro, D., Parks, W., Vidal, M., and Pagano, M. (1999). Identification of a family of human F-box proteins. Curr. Biol. *9*, 1177–1179.

Cho, H., Zhao, X., Hatori, M., Yu, R.T., Barish, G.D., Lam, M.T., Chong, L.-W., DiTacchio, L., Atkins, A.R., Glass, C.K., et al. (2012). Regulation of circadian behaviour and metabolism by REV-ERB-α and REV-ERB-β. Nature *485*, 123–127.

Dai, C., and Gu, W. (2010). p53 post-translational modification: deregulated in tumorigenesis. Trends Mol. Med. *16*, 528–536.

Dardente, H., Mendoza, J., Fustin, J.M., Challet, E., and Hazlerigg, D.G. (2008). Implication of the F-Box Protein FBXL21 in circadian pacemaker function in mammals. PLoS ONE *3*, e3530.

Gallego, M., and Virshup, D.M. (2007). Post-translational modifications regulate the ticking of the circadian clock. Nat. Rev. Mol. Cell Biol. *8*, 139–148.

Gekakis, N., Staknis, D., Nguyen, H.B., Davis, F.C., Wilsbacher, L.D., King, D.P., Takahashi, J.S., and Weitz, C.J. (1998). Role of the CLOCK protein in the mammalian circadian mechanism. Science *280*, 1564–1569.

Godinho, S.I., Maywood, E.S., Shaw, L., Tucci, V., Barnard, A.R., Busino, L., Pagano, M., Kendall, R., Quwailid, M.M., Romero, M.R., et al. (2007). The after-hours mutant reveals a role for Fbxl3 in determining mammalian circadian period. Science *316*, 897–900.

Hirano, A., Yumimoto, K., Tsunematsu, R., Matsumoto, M., Oyama, M., Kozuka-Hata, H., Nakagawa, T., Lanjakornsiripan, D., Nakayama, K.I., and Fukada, Y. (2013). FBXL21 regulates oscillation of the circadian clock through ubiquitination and stabilization of cryptochromes. Cell *152*, this issue, 1106–1118.

Hong, H.-K., Chong, J.L., Song, W., Song, E.J., Jyawook, A.A., Schook, A.C., Ko, C.H., and Takahashi, J.S. (2007). Inducible and reversible Clock gene expression in brain using the tTA system for the study of circadian behavior. PLoS Genet. *3*, e33.

Jin, J., Cardozo, T., Lovering, R.C., Elledge, S.J., Pagano, M., and Harper, J.W. (2004). Systematic analysis and nomenclature of mammalian F-box proteins. Genes Dev. *18*, 2573–2580.

Kerppola, T.K. (2006). Visualization of molecular interactions by fluorescence complementation. Nat. Rev. Mol. Cell Biol. *7*, 449–456.

Khan, S.K., Xu, H., Ukai-Tadenuma, M., Burton, B., Wang, Y., Ueda, H.R., and Liu, A.C. (2012). Identification of a novel cryptochrome differentiating domain required for feedback repression in circadian clock function. J. Biol. Chem. *287*, 25917–25926.

King, D.P., Zhao, Y., Sangoram, A.M., Wilsbacher, L.D., Tanaka, M., Antoch, M.P., Steeves, T.D., Vitaterna, M.H., Kornhauser, J.M., Lowrey, P.L., et al. (1997). Positional cloning of the mouse circadian clock gene. Cell *89*, 641–653.

Kondratov, R.V., Chernov, M.V., Kondratova, A.A., Gorbacheva, V.Y., Gudkov, A.V., and Antoch, M.P. (2003). BMAL1-dependent circadian oscillation of nuclear CLOCK: posttranslational events induced by dimerization of transcriptional activators of the mammalian clock system. Genes Dev. *17*, 1921–1932.

Lamia, K.A., Sachdeva, U.M., DiTacchio, L., Williams, E.C., Alvarez, J.G., Egan, D.F., Vasquez, D.S., Juguilon, H., Panda, S., Shaw, R.J., et al. (2009). AMPK regulates the circadian clock by cryptochrome phosphorylation and degradation. Science *326*, 437–440.

and + *Fbxl21*, > 24 hr. CRY1:R-10Ks half-life: alone, 6 hr; + *Fbxl3*, 1.8 hr; and + *Fbxl21*, 21 hr. CRY1:R-6Ks half-life: alone, 8.9 hr; + *Fbxl3*, 1.3 hr; and + *Fbxl21*, > 24 hr. CRY1:4Ks half-life: alone, 10.6 hr; + *Fbxl3*, 4.6 hr; and + *Fbxl21*, > 24 hr. Half-life parameter, K, is significantly different in all conditions, $p < 0.0001$, with the exception of the CRY1:R group.

(E) FBXL21-mediated CRY1 degradation via the K11 residue. Representative western blots of *Cry1*:R-K11-HA and *Cry1*:R-HA are shown. The experiment was performed as in (C). The K11 revertant underwent moderate degradation by FBXL21. K11 half-life: alone, > 24 hr; + *Fbxl3*, 18.4 hr; and + *Fbxl21*, 6.7 hr. Half-life parameter, K, for *Fbxl21* is significantly different: $p < 0.0001$. Data represent mean ± SEM.

(F) Eleven candidate CRY1 lysines subject to ubiquitination. All 31 lysine residues of CRY1 are shown, and candidate lysines for FBXL3- and FBXL21-mediated degradation are indicated with green and orange boxes, respectively.

(G) Differential roles of FBXL21 in nuclear and cytoplasmic CRY turnover. FBXL21 appears to form SCF complexes only in the cytoplasm and functions as a cytoplasmic-specific, weak E3 ligase for CRY degradation. In contrast, nuclear FBXL21 antagonizes FBXL3-mediated CRY degradation, thus conferring a CRY-protective function. In the absence of FBXL21, cytoplasmic CRY is stabilized, whereas in the nucleus CRY is destabilized because FBXL21 cannot antagonize the action of FBXL3. See also Figures S6 and S7 and Table S2.

Lee, C., Etchegaray, J.P., Cagampang, F.R., Loudon, A.S., and Reppert, S.M. (2001). Posttranslational mechanisms regulate the mammalian circadian clock. Cell *107*, 855–867.

Lowrey, P.L., and Takahashi, J.S. (2011). Genetics of circadian rhythms in Mammalian model organisms. Adv. Genet. *74*, 175–230.

Maywood, E.S., Chesham, J.E., Meng, Q.J., Nolan, P.M., Loudon, A.S., and Hastings, M.H. (2011). Tuning the period of the mammalian circadian clock: additive and independent effects of CK1εTau and Fbxl3Afh mutations on mouse circadian behavior and molecular pacemaking. J. Neurosci. *31*, 1539–1544.

Meng, Q.J., Logunova, L., Maywood, E.S., Gallego, M., Lebiecki, J., Brown, T.M., Sládek, M., Semikhodskii, A.S., Glossop, N.R., Piggins, H.D., et al. (2008). Setting clock speed in mammals: the CK1 epsilon tau mutation in mice accelerates circadian pacemakers by selectively destabilizing PERIOD proteins. Neuron *58*, 78–88.

Mohawk, J.A., Green, C.B., and Takahashi, J.S. (2012). Central and peripheral circadian clocks in mammals. Annu. Rev. Neurosci. *35*, 445–462.

Pines, J. (2011). Cubism and the cell cycle: the many faces of the APC/C. Nat. Rev. Mol. Cell Biol. *12*, 427–438.

Pines, J., and Lindon, C. (2005). Proteolysis: anytime, any place, anywhere? Nat. Cell Biol. *7*, 731–735.

Popov, N., Schülein, C., Jaenicke, L.A., and Eilers, M. (2010). Ubiquitylation of the amino terminus of Myc by SCF(β-TrCP) antagonizes SCF(Fbw7)-mediated turnover. Nat. Cell Biol. *12*, 973–981.

Preitner, N., Damiola, F., Lopez-Molina, L., Zakany, J., Duboule, D., Albrecht, U., and Schibler, U. (2002). The orphan nuclear receptor REV-ERBalpha controls circadian transcription within the positive limb of the mammalian circadian oscillator. Cell *110*, 251–260.

Reed, S.I. (2003). Ratchets and clocks: the cell cycle, ubiquitylation and protein turnover. Nat. Rev. Mol. Cell Biol. *4*, 855–864.

Siepka, S.M., Yoo, S.H., Park, J., Song, W., Kumar, V., Hu, Y., Lee, C., and Takahashi, J.S. (2007). Circadian mutant Overtime reveals F-box protein FBXL3 regulation of cryptochrome and period gene expression. Cell *129*, 1011–1023.

Tong, X., Buelow, K., Guha, A., Rausch, R., and Yin, L. (2012). USP2a protein deubiquitinates and stabilizes the circadian protein CRY1 in response to inflammatory signals. J. Biol. Chem. *287*, 25280–25291.

Ukai-Tadenuma, M., Yamada, R.G., Xu, H., Ripperger, J.A., Liu, A.C., and Ueda, H.R. (2011). Delay in feedback repression by cryptochrome 1 is required for circadian clock function. Cell *144*, 268–281.

van der Horst, G.T., Muijtjens, M., Kobayashi, K., Takano, R., Kanno, S., Takao, M., de Wit, J., Verkerk, A., Eker, A.P., van Leenen, D., et al. (1999). Mammalian Cry1 and Cry2 are essential for maintenance of circadian rhythms. Nature *398*, 627–630.

Vitaterna, M.H., Selby, C.P., Todo, T., Niwa, H., Thompson, C., Fruechte, E.M., Hitomi, K., Thresher, R.J., Ishikawa, T., Miyazaki, J., et al. (1999). Differential regulation of mammalian period genes and circadian rhythmicity by cryptochromes 1 and 2. Proc. Natl. Acad. Sci. USA *96*, 12114–12119.

Xu, M., Skaug, B., Zeng, W., and Chen, Z.J. (2009). A ubiquitin replacement strategy in human cells reveals distinct mechanisms of IKK activation by TNFalpha and IL-1beta. Mol. Cell *36*, 302–314.

Yagita, K., Tamanini, F., Yasuda, M., Hoeijmakers, J.H., van der Horst, G.T., and Okamura, H. (2002). Nucleocytoplasmic shuttling and mCRY-dependent inhibition of ubiquitylation of the mPER2 clock protein. EMBO J. *21*, 1301–1314.

Yoo, S.H., Yamazaki, S., Lowrey, P.L., Shimomura, K., Ko, C.H., Buhr, E.D., Siepka, S.M., Hong, H.K., Oh, W.J., Yoo, O.J., et al. (2004). PERIOD2: LUCIFERASE real-time reporting of circadian dynamics reveals persistent circadian oscillations in mouse peripheral tissues. Proc. Natl. Acad. Sci. USA *101*, 5339–5346.

Yoo, S.H., Ko, C.H., Lowrey, P.L., Buhr, E.D., Song, E.J., Chang, S., Yoo, O.J., Yamazaki, S., Lee, C., and Takahashi, J.S. (2005). A noncanonical E-box enhancer drives mouse Period2 circadian oscillations in vivo. Proc. Natl. Acad. Sci. USA *102*, 2608–2613.

Zheng, X., and Sehgal, A. (2012). Speed control: cogs and gears that drive the circadian clock. Trends Neurosci. *35*, 574–585.

EXTENDED EXPERIMENTAL PROCEDURES

Mouse Strains

C57BL/6J (Stock # 000664), BTBR T^{+} *tf/J* (Stock #002282) and C3H/HeJ (Stock # 000659) mice were purchased from the Jackson Laboratory (Bar Harbor, ME). All mice were housed under LD12:12 unless otherwise noted. All animal care and experimental treatments were in accordance with Northwestern University and UT Southwestern Medical Center guidelines for animal care and use.

Mutagenesis and Breeding Scheme to Produce Mutant Mice

N-Ethyl-*N*-nitrosourea (ENU) (Sigma N3385) was prepared as previously described (Siepka and Takahashi, 2005a; Siepka et al., 2007). To ensure accurate ENU dose delivery, ENU concentration was determined by OD spectroscopy where 1 OD = 0.72 mg/ml. Six-week old male C57BL/6J mice were injected with 90 or 100 mg/ kg body weight of ENU. After a 6-week recovery period, ENU treated mice were mated with wild-type C57BL/6J females to produce generation 1 (G1) males. A single G1 male is representative of one mutagenized gamete and was used as a kindred founder (Figure S1). G1 males were mated with wild-type C57BL/6J females to produce G2 females. Four G2 females were backcrossed to their G1 fathers to produce G3 mice for phenotyping. Five G3 mice from every G2 backcross (20 mice per kindred) were phenotyped to ensure an 85% probability of detecting a recessive mutation in the kindred. All mice in our production colony were housed under an LD12:12 cycle.

Measurement of Free-Running Period

Mice (6–10 weeks of age) were placed in individual running wheel cages and their activity recorded continuously using the ClockLab data collection system (Actimetrics, Evanston, IL) for 4 weeks in the ENU screen as described (Siepka and Takahashi, 2005b). After the first week on an LD12:12 cycle, the mice were released into constant darkness (DD) for the remaining 3 weeks. Free running periods were measured by line fitting of activity onsets from data collected during the DD period of the assay using ClockLab data analysis software. Experiments with Scg2::tTA X tetO::Psttm transgenic mice were conducted as described previously (Hong et al., 2007).

Heritability Testing

Putative mutants (or putants) were mated with wild-type C57BL/6J mice to produce G4 offspring. These G4 mice were intercrossed to produce G5 mice for phenotyping. All G3 mice that produced G5 mice with identical or more extreme phenotypes passed the heritability test and were considered true mutants.

DNA Extractions

DNA for genotyping was extracted from tail tip samples as follows: 2 mm tail tip samples were placed in 1.5 ml micro-centrifuge tubes and incubated in 100 ml 50 mM NaOH at 95°C (in a heating block) for 45 min. The extract was neutralized with 10 ml 1 M Tris-HCl (pH 5.0), vortexed briefly and micro-centrifuged at 10,000 rpm for 5 min to pellet cellular debris. The DNA containing supernatant was placed in a clean micro-centrifuge tube and stored at –20°C. DNA was diluted 1:10 in 10 mM Tris-HCl pH 8.0, 1 mM EDTA to create a working stock for PCR analysis.

Mutation Mapping

Psttm/*Psttm* male mice were mated to BTBR/J female mice to create [*Psttm*/+ x BTBR/J] F1 mice. The F1 progeny were intercrossed to produce 111 [(*Psttm*/+ x BTBR/J) x (*Psttm*/+ x BTBR/J)] F2 mice for mutation mapping. *Psttm*/*Psttm* male mice were also mated to C3H/HeJ female mice to create [*Psttm*/+ x C3H/HeJ] F1 mice. The F1 progeny were intercrossed to produce an additional 364 [(*Psttm*/+ x C3H/HeJ) x (*Psttm*/+ x C3H/HeJ)] F2 mice for mapping. Wheel running behavior of all mapping mice was analyzed as described above. Four of the 111 BTBR F2 mapping mice with the shortest period values (presumptive *Past-time* homozygotes by phenotype) selected and genotyped. The initial genotyping was performed at the Harvard Partners Genome Center, Cambridge, MA using an Illumina 768 SNP panel (~500 which are informative for our cross). Initially, *Psttm* was located by homozygosity mapping to a 40-Mb region of chromosome 13 (Figure S1B, C). DNA was extracted from tail tips from the affected BTBR F2 individuals as using a PureGene DNA extraction kit (QIAGEN) and analyzed as previously described (Moran et al., 2006). In the C3H X B6 F2 cross, 72 of the 364 mice were *Past-time* homozygotes confirmed by genotype using markers flanking the 40-Mb region.

Only *Past-time* homozygous mice (78 genotyped for a total of 156 meioses) were used for fine genetic mapping. The following SNP markers were used to narrow the *Past-time* genetic interval on chromosome 13: *rs13481788, rs13481798, rs29244502, rs4229759, rs29822615, rs30237987, rs29517854, rs29552064, rs29826980, rs6220659 and rs3679222.* SNP primer sets were designed using Primer3 software. The sequences of these primers sets are available from the authors by request. PCR reactions were carried out in 6 μl volumes using 10-25 ng template genomic DNA with 1x Master Mix for SYBR® Green (Part # 4309155, Applied Biosystems Inc, Foster City, CA), 5 pmoles each of forward and reverse primers in MicroAmp 96- or 384-well Optical Reaction Plates (Applied Biosystems, Inc.). Thermo-cycling reaction conditions were as follows: 40 cycles of 95°C for 15 s and 60°C for 30 s. Data were collected and analyzed with either an ABI Prism 7700 Sequence Detector or an ABI 7900HT Fast Real-Time PCR System (Applied Biosystems, Inc.).

DNA Sequencing

Sequencing was performed at the Harvard Partners Genome Center, Cambridge, MA. Genomic DNA was extracted from tail tips from one wild-type C57BL/6J mice and two different individual *Psttm/Psttm* mice as described above. All annotated exons from *Fbxl21* were amplified by PCR using genomic DNA templates. Most exons were small enough to be amplified and sequenced in a single amplicon (~600 bp). Some larger exons, however, were sequenced by multiple overlapping 600 bp amplicons. Sequencing data were analyzed using Poly Phred and Consed software.

Past-time Genotyping

Past-time alleles were detected by PCR mutagenesis that introduces an EcoRI restriction site into *Past-time* mutant samples while leaving the wild-type allele resistant to EcoRI. The reverse primer (60-mer) has one mismatched base at the 4th position from the 3′ end of the primer. This mismatch creates an EcoRI site in samples amplified from a *Past-time* DNA template. DNA from mutant mice was amplified (PCR product = 290 bp) and cut with EcoRI to generate 2 DNA fragments (229 and 61 bp). Wild-type template DNA does not generate an EcoRI site and remains intact after digestion. Following complete digestion, the amplified and EcoRI digested PCR products were separated on 3%–4% agarose gels. PCR reactions were carried out in 10 μl volumes using 10-25 ng genomic DNA template with 1x GoTaq PCR buffer (+ $MgCl_2$), 1 μmole each of forward (5′TGTGAGCTCAGACATTTTATATCAGA-3′') and reverse primer (5′ GACAACAGCACTCTTACCTTGGGCACCATGAAACTTGGTTTGGCTGTTGAAATgAAT-3′), 100 uM dNTP mix, 1 M Betaine and 0.01 units GoTaq (Promega Corporation, Madison, WI). Thermo-cycling reaction conditions were as follows: 95°C for 2 min, 30 cycles of 95°C for 15 s and 55°C for 30 s and 72°C for 15 min, followed by 72°C for 3 min. Restriction enzyme digestions were carried out in 25 μl volumes using the 10 μl PCR reaction in 1x EcoR1 buffer (New England Biolabs, Ipswich, MA) and 100 units of EcoR1. Reactions were incubated at 37°C for 2 hr. The resulting amplified and digested PCR products were separated on a 3% agarose/1% NuSieve gel in 1x TBE buffer and visualized by ethidium bromide staining.

Overtime Genotyping

Mice were genotyped for the *Overtime* mutation using real-time PCR to detect single nucleotide polymorphisms (SNPs) as described previously (Siepka et al., 2007). PCR reactions were carried out in 6 μl volumes using 10-25 ng template genomic DNA with 1x Master Mix for SYBR® Green (Part # 4309155, Applied Biosystems Inc, Foster City, CA) 5 pmoles each of forward (wild-type forward primer = 5′GTTGCAAAAATTTGTCAGCaAt-3′ or *Overtime* forward primer = 5′GTTGCAAAAATTTGTCAGCaAc-3′) and reverse primer (5′CCCCACACATCTTCACAAACT-3′) in MicroAmp 96- or 384-well Optical Reaction Plates (Applied Biosystems, Inc.). Thermo-cycling reaction conditions were as follows: 40 cycles of 95°C for 15 s and 60°C for 30 s. Data were collected and analyzed with either an ABI Prism 7700 Sequence Detector or an ABI 7900HT Fast Real-Time PCR System (Applied Biosystems, Inc.).

Immunoblotting and Immunoprecipitation

Immunoblotting and immunoprecipitation were performed as described previously (Siepka et al., 2007). For in vivo ubiquitination assay and nuclear fraction extraction, 6M urea containing lysis buffer [20 mM Tris pH 7.5, 150 mM NaCl, 1mM EDTA, 2mM EGTA, 1.5 mM MgCl2, 10 mM NaF, 2mM DTT, 0.5% Triton X-100, cocktail inhibitor (Roche)] was used. An antibody against PER1 was a generous gift from Dr. Choogon Lee. PER2 (epitope: aa 41-180), CRY1 (epitope: aa 496-606), CRY2 (epitope: aa 514-592), FBCL21-C (epitope: aa 404-420), FBXL21-N (epitope: aa 7-26), FBXL3 (epitope: aa 398-414) antibodies were generated using guinea pig or rabbit (Cocalico Biologicals) and serum was affinity purified using the same protein or peptide used to raise the antibody. Commercial vendors of antibodies used include Invitrogen (anti-Skp1, anti-Cullin1, anti-V5), Cell Signaling (anti-Myc), Santa Cruz (β- actin, α-tubulin), Sigma (anti-Flag), Abcam (anti-LaminB1), and Roche (anti-HA).

RNA Isolation and Real-Time PCR

RNA isolation and real-time PCR were performed as described previously (Siepka et al., 2007). For clock controlled genes from the liver RNA samples, a Fluidigm Biomark System and 48.48 real-time PCR plates along with ABI taqman probes (Mm00455950_m1 CLOCK, Mm00500226_m1 BMAL1, Mm00501813_m1 PER1, Mm00478113_m1 PER2, Mm00478120_m1 PER3, Mm00514392_m1 CRY1, Mm00546062_m1 Cry2, Mm00520708_m1 Rev-erb alpha, Mm00500848_m1 NPAS2, Mm00478593_m1 Dec1, Mm00470512_m1 Dec2, Mm01194021_m1 Dbp) were used according to the manufacturer's instructions.

Circadian Bioluminescence Experiments

WT *mPer2::Luc* mice (Yoo et al., 2004) or *Psttm/Psttm* X *mPer2::Luc* mice were euthanized by cervical dislocation between ZT11 and ZT12.5. SCN tissues were isolated from 300 μm coronal sections, and pituitary tissues were dissected and kept in chilled Hanks' buffered salt solution (Invitrogen). All dissected tissues were cultured on Millicell culture membranes (PICMORG50, Millipore) and were placed in 35 mm tissue culture dishes containing 2 ml DMEM media (Mediatech) supplemented with 352.5 μg/ml sodium bicarbonate, 10 mM HEPES (Invitrogen), 2 mM L-Glutamine, 2% B-27 Serum-free supplement (Invitrogen), 25 units/ml penicillin, 25 μg/ml streptomycin (Invitrogen), and 0.1mM luciferin potassium salt (L-8240, Biosynth AG). Sealed dishes were placed in LumiCycle luminometer machines (Actimetrics, Wilmette, IL) and bioluminescence was recorded continuously. For MEF cell bioluminescence measurement, B27 was replaced with 2% FBS.

In Vitro Ubiquitination Assays

CRY1 containing SCF complex was purified from Sf9 cells (Invitrogen) using M2 FLAG agarose. Ubiquitination of CRY1 was carried out in buffer containing 20 mM HEPES, pH7.5, 2 mM ATP, 5 mM $MgCl_2$ and 0.2 mM DTT for 1 hr at 30°C. The reaction mixture contained 10 μg/ml E1, 10 μg/ml E2 UbcH5c or 10 μg/ml His6-Ubc13/His6-Uev1A, 0.5 mg/ml ubiquitin (Boston Biochem). The reaction were stopped by adding 2X SDS loading buffer and analyzed by Western blotting with an anti-Myc antibody.

Cell Culture and Transfection

WT, *Psttm,* WT *mPer2::Luc* and *Psttm mPer2::Luc* MEF cells were isolated from 13.5 day mouse embryos. NIH 3T3 and 293A cells were cultured in DMEM (Mediatech) supplemented with 10% fetal bovine serum. For immunoprecipitations, 1×10^6 cells were plated into the 100 mm dishes 1 day before transfection, Effectene reagent (QIAGEN) was used to transfect DNA according to the manufacturer's protocol. CRY degradation assays were performed by transfecting *Cry1 or Cry2* with or without *Fbxl3*, *Fbxl21*, *Psttm* constructs into 2×10^5 293A cells in 12 well plate. Thirty-six hours after transfection 20 ug/ml (WT *Cry1/2*) or 100ug/ml (*Cry1:R*) cycloheximide (CHX) was added and cells collected at the indicated time. siRNA for *Fbxl3* was purchased from Dharmacon and transfection was performed by using Lipofectamine 2000 (Invitrogen). For the luminescence assay, 293A cells were plated the day before transfection at 2×10^5 cells per well in 6-well plates. Cells were transfected with indicated vectors by using Effectene reagent. Forty-eight hours after transfection, cells were lysed and luminescence was measured from 20 μl of lysate in the Luciferase Assay System (Promega) using a luminometer (AutoLumet Plus; Berthold Technologies).

Plasmids and Small Hairpin RNAs

Mouse *Fbxl21* cDNA was synthesized from C57BL/6J heart total RNA and cloned into pCMV10-3XFlag vector (Sigma). Site directed mutagenesis was performed to generate the *Psttm* mutation from the wild-type cDNA (5′- CTATCCAGACCTTGGAATTGATTTCAA CAGC, 5′- GCTGTTGAAATCAATTCCAAGGTCTGGATAG). pTRE2 (Clontech) vector was used to generate the vector for tetO::*Psttm* transgenic animals. cDNAs encoding m*Cry1*, m*Fbxl3*, m*Fbxl21*, *Psttm*, h*Cullin1*, h*Rbx1*, h*Skp1* were cloned into the baculoviral expression vector pFastBac HTa (Invitrogen). mCry1 C-terminal truncated vector was generated using following primers: B-Cry1CTD 5′-GGGGACCACTTTGTACAAGAAAGCTGGGTACTAATTCCCGCTGCTGCTACA, C-Cry1CTD 5′-GGGGACCACTTTGTACAAGAAA GCTGGGTACTAATTTCCACCGCTACAGCT, D-Cry1CTD 5′-GGGGACCACTTTGTACAAGAAAGCTGGGTACTAGAGTGAGTGAGT CTGCTG, F-Cry1CTD 5′-GGGGACCACTTTGTACAAGAAAGCTGGGTACTAGGGGCCGACACTCTGGGC.

ATCCTCTTCC. shRNA vectors targeting mouse *Fbxl21* were constructed using a previously described method (Xu et al., 2009) and transfected into WT MEF cells and clonal selection was performed under 2ug/ml puromycin. The oligonucleotides used to construct the shRNA for mouse *Fbxl21* are as follows: siFbxl21-1F, 5′-GATCCCTTGTCAACTCAAAATCGTTTTCAAGAGAAACGATTTTGAG TTGTCTTTTTTTA-3′; siFbxl21-1R, 5′-AGCTTAAAAATTGTCAACTCAAAATCGTTTCTCTTGAAAACGATTTTGAGTTGTCTTGG-3′; siFbxl21-2F, 5′-GATCCCCCGTCACTCACCTTTATTTTTCAAGAGAAAATAAAGGTGAGTGACGGTTTTTA-3′; siFbxl21-2R, 5′-AGCTT AAAAACCGTCACTCACCTTTATTTTCTCTTGAAAAATAAAGGTGAGTGACGGGG-3′; siFbxl21-3F, 5′-GATCCCCGATTAAAATTGA GGACACTTCAAGAGAGTGTCCTCAATTTTAATCGTTTTTA-3′; siFbxl21-3R, 5′-AGCTTAAAAACGATTAAAATTGAGGACACTCTC TTGAAGTGTCCTCAATTTTAATCGGG-3′; siFbxl21-4F, 5′-GATCCCGGAGGAAGTTTGAGTTTGATTCAAGAGATCAAACTCAAAC TTCCTCCTTTTTA-3′; siFbxl21-4R, 5′-AGCTTAAAAAGGAGGAAGTTTGAGTTTGATCTCTTGAATCAAACTCAAACTTCCTCCGG-3′.

For lentivirus production, m*Fbxl21*shRNA (4 copy) fragment was cloned into the pFUW Lentivirus vector. Lentivirus vectors containing m*Fbxl21* shRNA were co-transfected with packaging vectors into HEK293T cells (ATCC) using Lipofectamine 2000 (Invitrogen). A total of 10 μg of DNA was used, including 6 μg of the pFUW vector or m*Fbxl21* shRNA vectors, 3 μg of Δ8.9 and 1 μg of V-SVG. Virus particles were harvested twice after transfection, at 48 and 72 hr respectively, and passed through a 0.45 μm low protein binding syringe filter. The filtrate was supplemented with 8 μg/ml polybrene and added to 10 cm plates containing a clonal line of immortalized fibroblasts derived from mPER2::LUC knock-in mice ($2x10^6$ fibroblasts). Forty-eight hours following the second addition of virus, the transduced fibroblasts were sorted by FACS to select only GFP positive cells. Collected cells were expanded and then subcultured into 35 mm dishes for circadian time point collection and for real-time mPER2::LUC bioluminescence measurements using a LumiCycle apparatus (Actimetrics, Wilmette, IL).

Nuclear Fractionation

MEF cells ($8X10^5$/60mm dish) were plated two to three days before synchronization with Dexamethasone (0.2 μM). For the protein half-life measurement experiments, 32-36 hr after synchronization, cells were treated with 100 ug/ml CHX for the indicated times, washed with PBS and harvested. Cell pellets were resuspended in 5 volumes of Buffer A (hypotonic; 10 mM HEPES (pH7.9), 0.2 mM EDTA, 0.2 mM EGTA, 1 mM DTT, 1 mM PMSF, 10 mM NaF, 1 mM Na_3OV_4, Complete mini, Roche) and incubated on ice for 10 min. Triton X-100 was added to the final concentration of 0.1% and vortexed for 15 s. Samples were centrifuged at 4,000 rpm for 5 min to obtain the supernatant (cytoplasmic fraction). The pellets were washed once with Buffer A and frozen. The pellets were resuspended in 6 M Urea extraction buffer (6 M Urea, 20 mM Tris pH 7.5, 150 mM NaCl, 1 mM EDTA, 1 mM EGTA, 1.5 mM $MgCl_2$, 10 mM NaF, 2 mM DTT, 0.5% Triton X-100, 1 mM Na_3OV_4, Complete mini, Roche) and centrifuged at 12000 rpm for 10 min to obtain the nuclear fraction.

Cry1 Mutants

The *Cry1:R* mutant in which all 31 lysine residues were mutated to arginine was synthesized by DNA2.0, Inc. (Menlo Park, CA). The *Cry1:R* sequence was codon optimized for baculovirus expression (*Spodoptera frugiperda* genomic codon bias). Site-directed mutagenesis of *Cry1:R* to construct lysine revertant clones was performed using the primers in Table S2.

Bimolecular Fluorescence Complementation (BiFC) Assay

Full-length Venus (Ex515/Em528) and Cerulean (Ex433/Em475) have been described previously (Meyer et al., 2006). Based on published reports (Hu et al., 2002; Hu and Kerppola, 2003), truncated Venus and Cerulean fragments in the pEGFP-C1 (Clontech) backbone were created as CerN (1-155 aa), CerC (156-239 aa), VenN (1-155 aa) and VenC (156-239 aa) by site-directed mutagenesis PCR. PCR-amplified cDNAs corresponding to *Fbxl3, Fbxl21, Psttm, Ovtm, Cullin* or *Skp1* were inserted into the KpnI and SmaI restriction sites downstream of the coding region of Venus, VenN and VenC. Likewise, CerN was attached to the N-terminus of *Fbxl3, Fbxl21* and *Psttm* via the same strategy. PCR-amplified *Cry1* cDNA was inserted into the NheI and AgeI sites upstream of the coding region of CerC and VenC.

For localization experiments, 25 ng of the nuclear marker H2B-mRFP1 (Ex584/Em607) (Li et al., 2007) was mixed with 50 ng Venus-tagged *Fbxl* or *Cry1*, and 150 ng of pCDNA-E2-Eluc. For Venus BiFC experiments, 25 ng H2B-mRFP1 was mixed with 100 ng VenN-*Fbxl* and 100 ng *Cry1*-VenC, VenC-*Skp1* or VenC-*Cullin*. $3x10^5$ HEK293A cells were suspended in DMEM supplemented with 10% FBS when transfected with 225 ng DNA by using the Effectene kit (QIAGEN), and plated into a well of a 24-well black Visiplate (Perkin-Elmer). Medium was changed after overnight incubation at 37°C, 5% CO_2. Plates were washed with PBS once 2 days after transfection and fixed with 4% paraformaldehyde in PBS for 15 min. Samples were stained with DAPI (1 ug/ml), washed twice, immersed with PBS and sealed with top-seal A membrane (Perkin-Elmer). For BiFC competition experiments, 25 ng H2B-mRFP1 was mixed with 50 ng *Cry1*-CerC and 75 ng *Fbxl* BiFC plasmid carrying VenN or CerN.

Fluorescence images were acquired on a Deltavision Personal DV Imaging System (Applied Precision) equipped with an inverted 20x 0.45NA UPLFL objective and a Microtiter stage on an Olympus IX71 microscope. Four locations in each well were selected and autofocused with RFP1 fluorescence. 12-layer Z stacks with 1 μm steps were scanned in the channel sequence of YFP (Ex513/17; Em559/34), CFP (Ex438/24; Em465/30), RFP (Ex575/25; Em632/60) and DAPI (Ex390/18; Em435/40) filter sets with the Z step first. Image stacks were deconvoluted with the Softworx (Applied Precision) deconvolution module and maximal intensity Z projections of layers were built.

For quantification of BiFC competition results, original image files were imported to and organized by ImageJ (NIH), and exported image sequences were pushed through a custom pipeline run by Cellprofiler (Broad Institute). Briefly, the nuclei were first recognized based on RFP fluorescence, and then inverse-masked with strong aggregates in the Venus channel. Mean Venus intensity value of each masked nucleus was measured. About 40-70 cells were identified and measured in each image, and the average values of cells in one image were obtained for further normalization and statistical analysis. Four images from each well were averaged and the experiments were replicated three times.

SUPPLEMENTAL REFERENCES

Hong, H.-K., Chong, J.L., Song, W., Song, E.J., Jyawook, A.A., Schook, A.C., Ko, C.H., and Takahashi, J.S. (2007). Inducible and reversible Clock gene expression in brain using the tTA system for the study of circadian behavior. PLoS Genet. *3*, e33.

Hu, C.D., and Kerppola, T.K. (2003). Simultaneous visualization of multiple protein interactions in living cells using multicolor fluorescence complementation analysis. Nat. Biotechnol. *21*, 539–545.

Hu, C.D., Chinenov, Y., and Kerppola, T.K. (2002). Visualization of interactions among bZIP and Rel family proteins in living cells using bimolecular fluorescence complementation. Mol. Cell *9*, 789–798.

Li, Y., Yu, W., Liang, Y., and Zhu, X. (2007). Kinetochore dynein generates a poleward pulling force to facilitate congression and full chromosome alignment. Cell Res. *17*, 701–712.

Meyer, P., Saez, L., and Young, M.W. (2006). PER-TIM interactions in living Drosophila cells: an interval timer for the circadian clock. Science *311*, 226–229.

Moran, J.L., Bolton, A.D., Tran, P.V., Brown, A., Dwyer, N.D., Manning, D.K., Bjork, B.C., Li, C., Montgomery, K., Siepka, S.M., et al. (2006). Utilization of a whole genome SNP panel for efficient genetic mapping in the mouse. Genome Res. *16*, 436–440.

Siepka, S.M., and Takahashi, J.S. (2005a). Forward genetic screens to identify circadian rhythm mutants in mice. Methods Enzymol. *393*, 219–229.

Siepka, S.M., and Takahashi, J.S. (2005b). Methods to record circadian rhythm wheel running activity in mice. Methods Enzymol. *393*, 230–239.

Siepka, S.M., Yoo, S.H., Park, J., Song, W., Kumar, V., Hu, Y., Lee, C., and Takahashi, J.S. (2007). Circadian mutant Overtime reveals F-box protein FBXL3 regulation of cryptochrome and period gene expression. Cell *129*, 1011–1023.

Xu, M., Skaug, B., Zeng, W., and Chen, Z.J. (2009). A ubiquitin replacement strategy in human cells reveals distinct mechanisms of IKK activation by TNFalpha and IL-1beta. Mol. Cell *36*, 302–314.

Yoo, S.H., Yamazaki, S., Lowrey, P.L., Shimomura, K., Ko, C.H., Buhr, E.D., Siepka, S.M., Hong, H.K., Oh, W.J., Yoo, O.J., et al. (2004). PERIOD2:LUCIFERASE real-time reporting of circadian dynamics reveals persistent circadian oscillations in mouse peripheral tissues. Proc. Natl. Acad. Sci. USA *101*, 5339–5346.

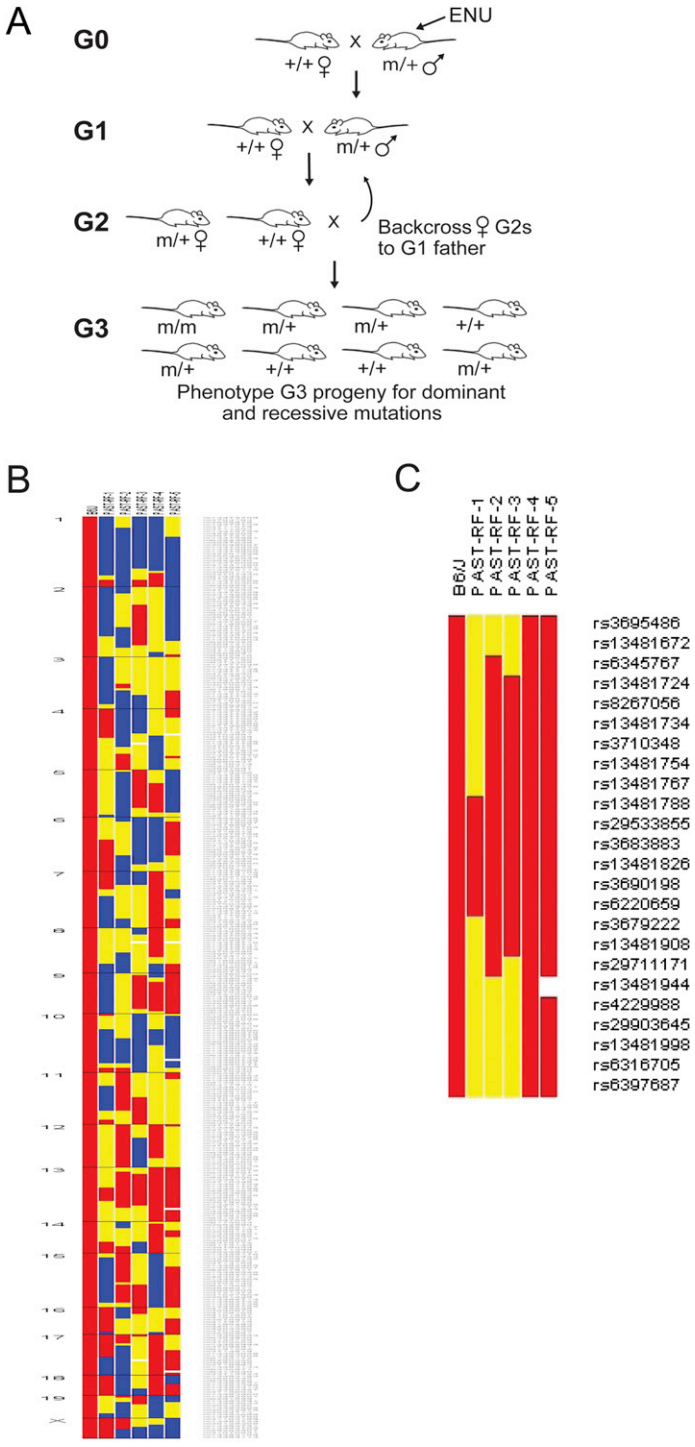

Figure S1. ENU Mutagenesis Screen, Related to Figure 1

(A) Mutant mouse production. Male C57BL/6J mice were exposed to the mutagen ENU, and mated with females 6-8 weeks post-injection to produce G1 mice. G1 males were mated to wild-type C57BL/6J females to produce G2 females that were then backcrossed to the G1s to produce G3 mice for phenotyping.

(B) *Past-time* was mapped by homozygosity using BTBR F2 mapping mice to a 40 Mb region of chromosome 13. Red, blue and yellow represent C57BL6/J, BTBR T^{+} *tf/J* and heterozygous alleles, respectively, for each SNP in the mapping panel.

(C) An enlarged representation of the mouse Chromosome 13 region containing the *Past-time* mutation.

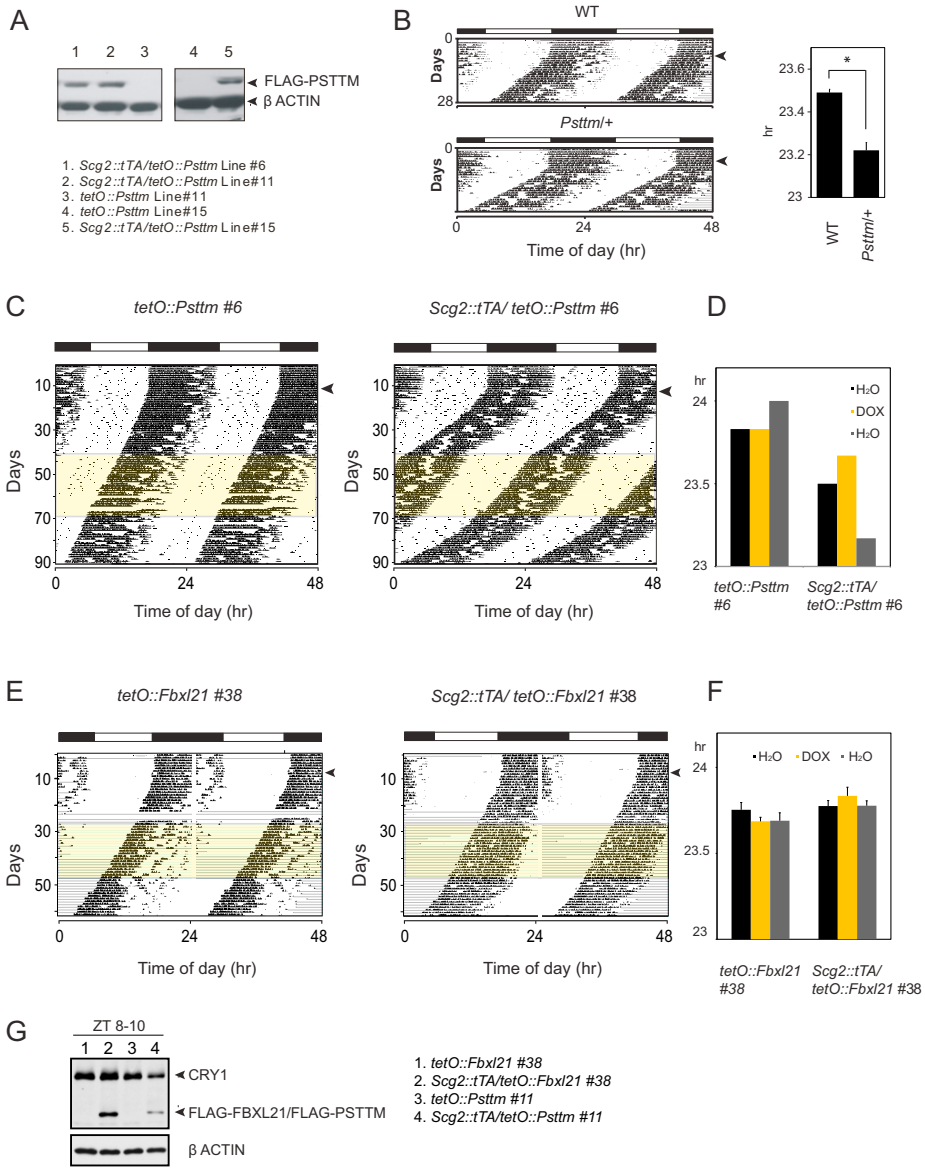

Figure S2. Characterization of *Psttm*, Related to Figure 2

(A) Western blotting results from single (*tetO::Psttm*) or double (*Scg2::tTA/tetO::Psttm*) transgenic mice. Anti-FLAG antibody was used to detect FLAG-PSTTM in cerebellum lysates. PSTTM expression was detected only in double-transgenic mice (lanes 1, 2, and 5).

(B) Representative actograms and average period length of *wild-type* and *Psttm*/+ F2 mice [mean period: WT 23.49 hr, SEM 0.0152 (n = 83), *Psttm*/+ 23.22 hr, SEM 0.0365 (n = 72), t test: **p*-value < 0.0001]. The actograms are double plotted where each horizontal line represents 48 hr of activity. The mice were kept on LD12:12 (represented in the bar above the actogram) for the first 7 days of the assay and then released into constant darkness for 21 days (indicated by the arrowhead on the right).

(C) Left panel: Representative actogram of tetO::*Psttm* line #6 single-transgenic mouse. Right panel: Representative actogram of a *Scg2::tTA*/tetO::*Psttm* line #6 double-transgenic mouse. Arrowheads indicate LD to DD transition. Doxycycline-containing water was administered during the period indicated by yellow boxes.

(D). Free running periods of single and double-transgenic mice during constant darkness with water (black), DOX water (yellow), and water after DOX treatment (gray).

(E) Left panel: Representative actogram of tetO::*Fbxl21* #38 single-transgenic mouse. Right panel: Representative actogram of a *Scg2::tTA*/tetO::*Fbxl21* #38 double-transgenic mouse. Arrowheads indicate LD to DD transition. Doxycycline-containing (10 μg/ml) water was administered during the interval indicated by yellow shading on the actogram.

(F) Free-running periods of single and double-transgenic mice during constant darkness with water (black), DOX (yellow), and water after DOX treatment (gray). Error bars show SEM (*tetO::Fbxl21 #38* n = 3, *Scg2::tTA/tetO::Fbxl21 #38* n = 5; There are no significant differences in period between genotype and treatment based on Bonferroni corrected pair-wise comparison).

(G) Western blotting results from single or double-transgenic mice. Anti-CRY1 and anti-FLAG antibodies were used to detect CRY1 and FLAG-FBXL21/PSTTM in cerebellum lysates respectively.

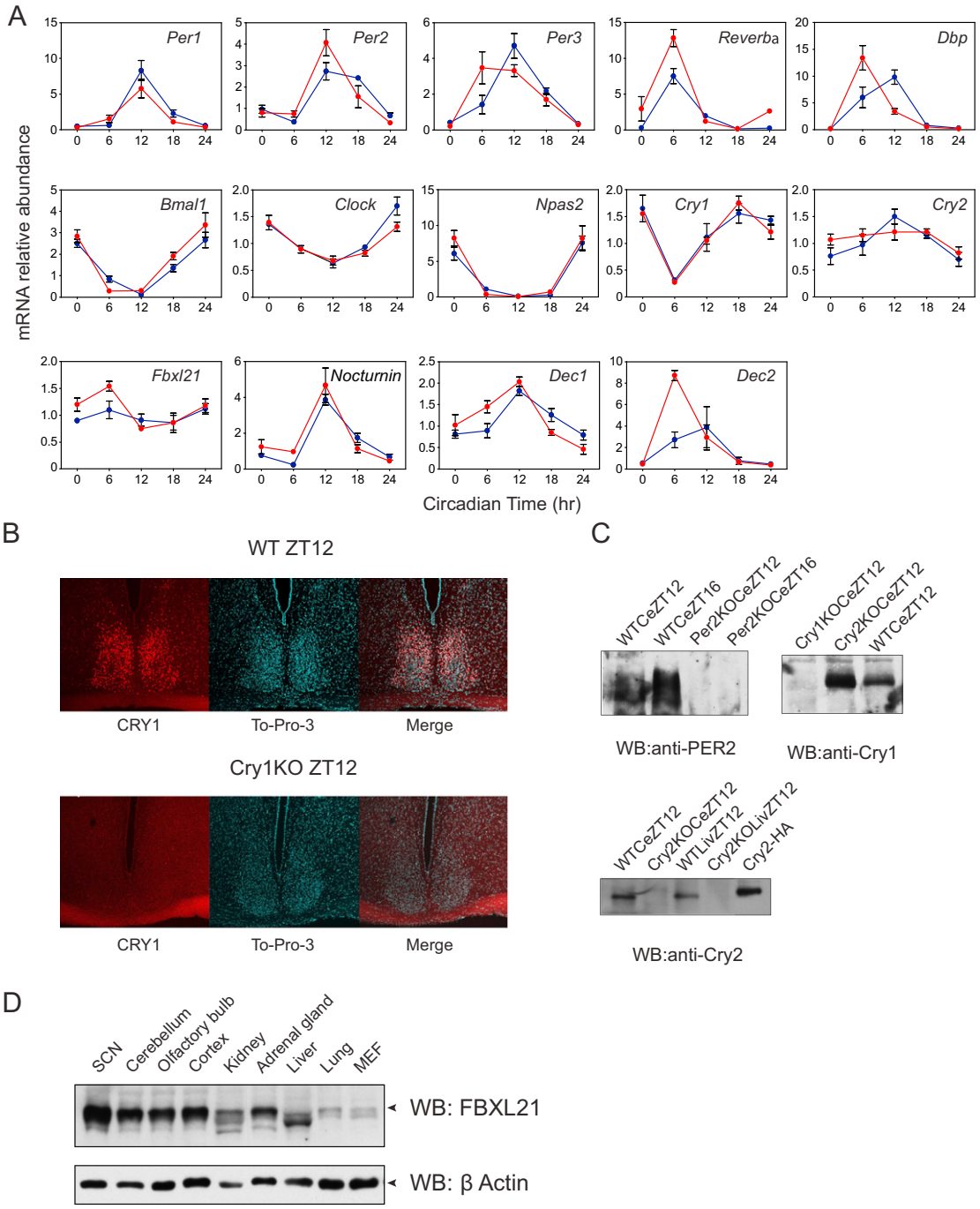

Figure S3. Effects of *Psttm* on Clock Gene Expression, Related to Figure 3

(A) Enhanced amplitude and advanced phase of clock genes in the liver of *Psttm* mice. Results from real-time RT-PCR (Fluidigm) analysis of clock gene expression in wild-type and *Psttm* mice are shown. Liver tissues from wild-type and *Psttm* mice were collected at the indicated circadian times. Filled and open circles represent WT and *Psttm* mice respectively. Error bars represent SEM for each time point from four independent repeats. Two-way ANOVA shows significant statistical differences between WT and *Psttm* mutant for *Per2* (CT12 $p < 0.05$), *Per3* (CT6, $p < 0.05$), *Reverbα* (CT6, $p < 0.001$), *Dbp* (CT6, CT12, $p < 0.001$), and *Dec2* (CT6, $p < 0.0001$).

(B) Immunocytochemical staining of SCN slices from *WT* and *Cry1* Knockout mice. CRY1 proteins were labeled with an anti-CRY1 antibody in coronal SCN sections. Representative images from ZT12 are shown. TO-PRO-3 was used for nuclear counterstaining.

(C) Antibody Characterization. The specificity of anti-PER2 (Guinea pig), anti-CRY1 (Guinea pig), anti-CRY2 (Guinea pig) antibodies were tested using tissue lysates from WT and corresponding knock-out mice.

(D) Western blot showing varying levels of endogenous FBXL21 levels in different mouse tissues at ZT12. Anti-FBXL21-C was used to detect FBXL21.

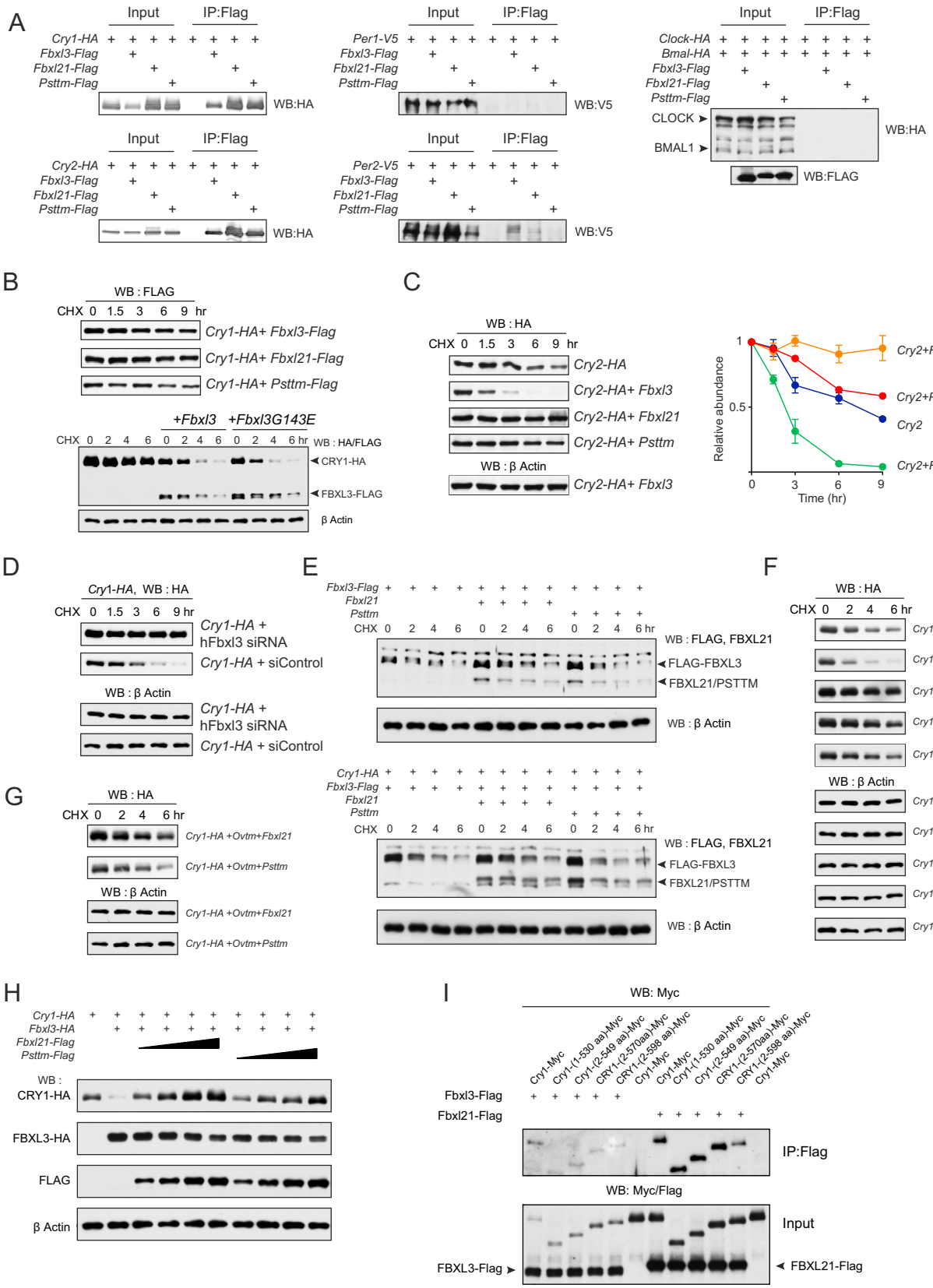
A
Input
IP:Flag
Cry1-HA
Fbxl3-Flag
Fbxl21-Flag
Psttm-Flag
WB:HA
Per1-V5
WB:V5
Clock-HA
Bmal-HA
CLOCK
BMAL1
WB:FLAG
Cry2-HA
Per2-V5
B
WB : FLAG
CHX 0 1.5 3 6 9 hr
Cry1-HA+ Fbxl3-Flag
Cry1-HA+ Fbxl21-Flag
Cry1-HA+ Psttm-Flag
+Fbxl3
+Fbxl3G143E
CHX 0 2 4 6 0 2 4 6 0 2 4 6 hr
WB : HA/FLAG
CRY1-HA
FBXL3-FLAG
β Actin
C
WB : HA
CHX 0 1.5 3 6 9 hr
Cry2-HA
Cry2-HA+ Fbxl3
Cry2-HA+ Fbxl21
Cry2-HA+ Psttm
WB : β Actin
Cry2-HA+ Fbxl3
Relative abundance
Time (hr)
Cry2+Fbxl21
Cry2+Psttm
Cry2
Cry2+Fbxl3
D
Cry1-HA, WB : HA
CHX 0 1.5 3 6 9 hr
Cry1-HA + hFbxl3 siRNA
Cry1-HA + siControl
WB : β Actin
E
Fbxl3-Flag
Fbxl21
Psttm
CHX 0 2 4 6 0 2 4 6 0 2 4 6 hr
WB : FLAG, FBXL21
FLAG-FBXL3
FBXL21/PSTTM
WB : β Actin
Cry1-HA
F
WB : HA
CHX 0 2 4 6 hr
Cry1-HA
Cry1-HA +Fbxl3
Cry1-HA +Fbxl21
Cry1-HA +Fbxl3+Fbxl21
Cry1-HA +Fbxl3+Psttm
WB : β Actin
G
WB : HA
CHX 0 2 4 6 hr
Cry1-HA +Ovtm+Fbxl21
Cry1-HA +Ovtm+Psttm
WB : β Actin
H
Cry1-HA
Fbxl3-HA
Fbxl21-Flag
Psttm-Flag
WB : CRY1-HA
FBXL3-HA
FLAG
β Actin
I
WB: Myc
Cry1-Myc
Cry1-(1-530 aa)-Myc
Cry1-(2-549 aa)-Myc
CRY1-(2-570aa)-Myc
CRY1-(2-598 aa)-Myc
Fbxl3-Flag
Fbxl21-Flag
IP:Flag
WB: Myc/Flag
Input
FBXL3-Flag
FBXL21-Flag

Figure S4. Characterization of FBXL21/PSTTM E3 Ligase Activity for CRY, Related to Figure 4

(A) FBXL21 and PSTTM bind selectively to CRY1/2 among the core clock proteins. 293A cells were transfected with the indicated combination of constructs (*Cry1-HA, Cry2-HA, Per1-V5, Per2-V5, Clock-HA, Bmal-HA*) together with the *Fbxl* expression constructs. Thirty-six hrs after transfection, cells were harvested and immunoprecipitations were performed using M2-Flag agarose. Both CRY1 and CRY2 were enriched by FBXL3, FBXL21, and PSTTM immunoprecipitation. PER1, CLOCK, and BMAL1 showed no detectable interaction with any of these F-box proteins. PER2 showed a weak signal in the immunoprecipitation, but the signal was not enriched relative to the input so we interpret the PER2 interaction to occur indirectly via CRY.

(B) Top panel: Western blotting (anti-FLAG) of F-box proteins from the samples in Figure 4D. Bottom panel: The *Psttm* mutation on *Fbxl3* (G143E) shows no effect on protein stability and CRY1 degradation activity of FBXL3. 293A cells were transfected with *Cry1-HA* alone or co-transfected with indicated *Fbxl3-Flag* constructs. Thirty-two hrs after transfection, cells were treated with 20 μg/ml CHX and incubated for the indicated time before harvest. Western blotting was performed to monitor CRY1 level (anti-HA) and FBXL3 level (anti-FLAG).

(C) Left panel: Differential effect of *Fbxl3*, *Fbxl21* and *Psttm* on CRY2 stability. 293A cells were co-transfected with *Cry2-HA* and *Flag-Fbxl3*, *Flag-Fbxl21* or *Flag-Psttm* constructs. Thirty-two hrs after transfection, cells were treated with 20 μg/ml cycloheximide and incubated for the indicated time before harvest. Western blotting was performed to monitor CRY2 levels using an anti-HA antibody. Right panel: Quantification of the effects of *Fbxl3*, *Fbxl21*, *Psttm* on CRY2 stability. Data represent three independent experiments. Error bars show ± SEM (n = 3). Blue: *Cry2* only; green: *Cry2* with *Fbxl3*; orange: *Cry2* with *Fbxl21*; red: *Cry2* with *Psttm*. CRY2 degradation was significantly enhanced or reduced in the presence of FBXL3 or FBXL21 respectively. *Psttm* was less effective compared with the wild-type *Fbxl21* in attenuating CRY2 degradation.

(D) Knockdown of *Fbxl3* in 293A cells stabilized CRY1. 293A cells were co-transfected with *Cry1*-HA and *hFbxl3* siRNA or scrambler siRNA (Dharmacon). Thirty-six hrs after transfection, cells were treated with 20 μg/ml cycloheximide and incubated for the indicated time before harvest. Western blotting was performed to monitor CRY1 levels using an anti-HA antibody.

(E) FBXL21 and PSTTM showed no obvious effect on FBXL3 stability. 293A cells were co-transfected with indicated constructs. Cycloheximide treatment was performed as in (C). Western blotting was performed to monitor FBXL3, FBXL21/PSTTM levels using an anti-Flag antibody and anti-FBXL21 respectively.

(F) Competition between FBXL3 and FBXL21/PSTTM in CRY1 degradation. Representative Western blots are shown for Figure 4F, top panel. 293A cells were transfected with *Fbxl3*, *Fbxl21*, *Fbxl3+Fbxl21*, or *Fbxl3+Psttm* constructs along with *Cry1*. Cycloheximide treatment and CRY1 Western blotting were performed as in (C).

(G) Competition between OVTM and FBXL21/PSTTM in CRY1 degradation. Representative Western blots are shown for Figure 4F, bottom panel. 293A cells were transfected with *Ovtm+Fbxl21*, *Ovtm+Psttm* constructs along with *Cry1*. Cycloheximide treatment and CRY1 Western blotting were performed as in (C).

(H) Competition between FBXL3 and FBXL21/PSTTM occurs in a dose-dependent manner. 293 A cells were transfected with indicated construct. Thirty two hrs after transfection Western blotting was performed to monitor CRY1, FBXL3, and FBXL21/PSTTM levels.

(I) FBXL3 and FBXL21 bind to the photolyase homology domain of CRY1 (1-530 aa). CRY1 C-terminal truncated constructs were co-transfected with *Fbxl3* or *Fbxl21* in 293A cells. Thirty two hrs after transfection, Immunoprecipitation was performed using M2 agarose beads. Immunoprecipitated proteins were analyzed by Western blotting with anti-Myc. Shorter truncation constructs within the photolyase homology domain were unstable.

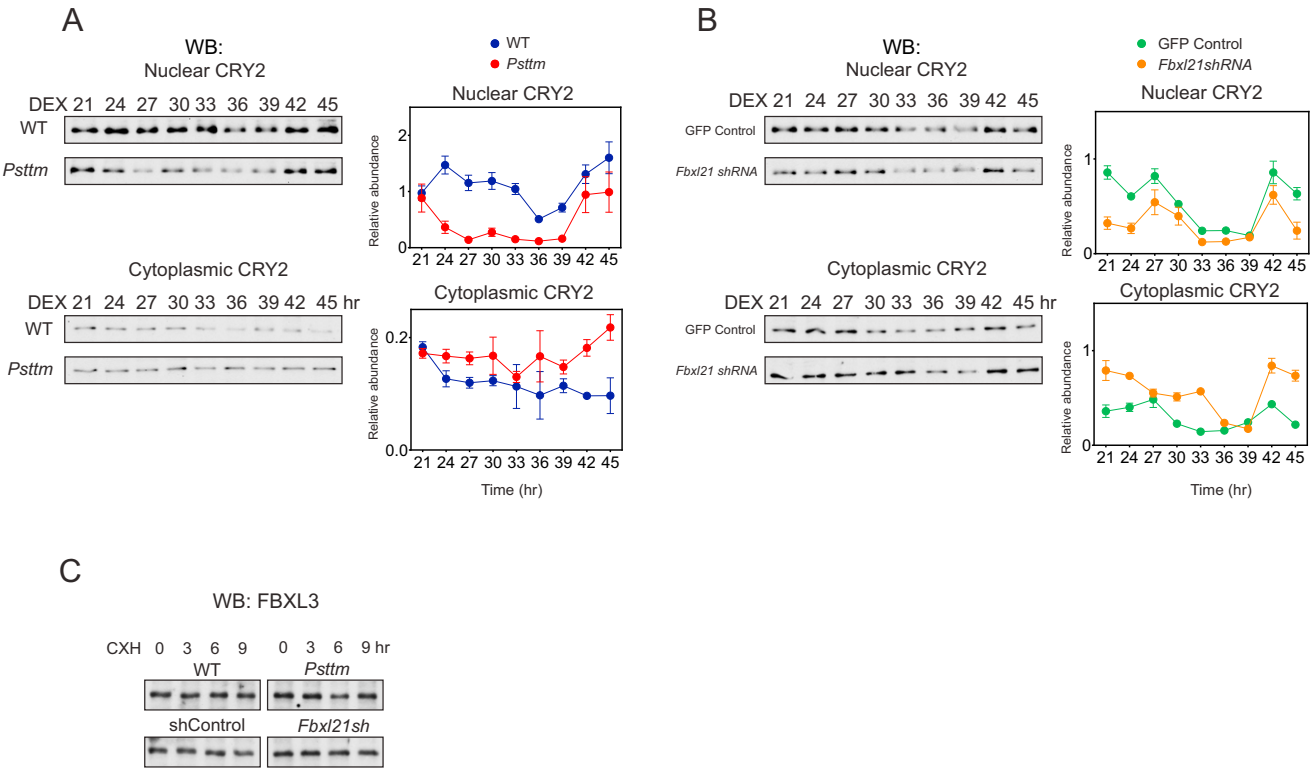

Figure S5. Differential Roles of FBXL21 in Nuclear and Cytoplasmic CRY2 Degradation, Related to Figure 5

(A) Left panel: The *Psttm* mutation reduces nuclear CRY2 level. WT and *Psttm* MEFs were plated two days before synchronization with Dexamethasone (0.2 μM). Nuclear and cytoplasmic fractions were collected at the indicated times. Western blotting was performed using nuclear and cytoplasmic fractions using an anti-CRY2 antibody. Right panels: Quantifications from triplicates including those shown in the example. Error bars show ± SEM (n = 3). In the top panel, CRY2 levels from *Psttm* nuclei (red) were significantly reduced compared to WT (blue) (two-way ANOVA, $p < 0.001$). In contrast, cytoplasmic CRY2 levels were significantly increased throughout the circadian cycle (red, bottom panel).

(B) Left panel: *Fbxl21* knockdown revealed *Psttm* is a loss-of-function mutation for CRY2 degradation. Lenti-GFP and Lenti-*Fbxl21sh* infected mPER2::LUC MEFs were treated the same as in (A). In the nucleus CRY2 level and oscillation amplitude were reduced similar to that seen in *Psttm* MEFs. Right panels: Quantifications from triplicates including those shown in the example. Error bars show ± SEM (n = 3). CRY2 levels in Lenti-*Fbxl21sh* nuclei were significantly reduced (orange, top panel) relative to GFP control (green), whereas cytoplasmic CRY2 levels were significantly increased throughout the circadian cycle (orange, bottom panel).

(C) The *Psttm* mutation or depletion of endogenous FBXL21 did not have any effect on nuclear FBXL3 protein levels.

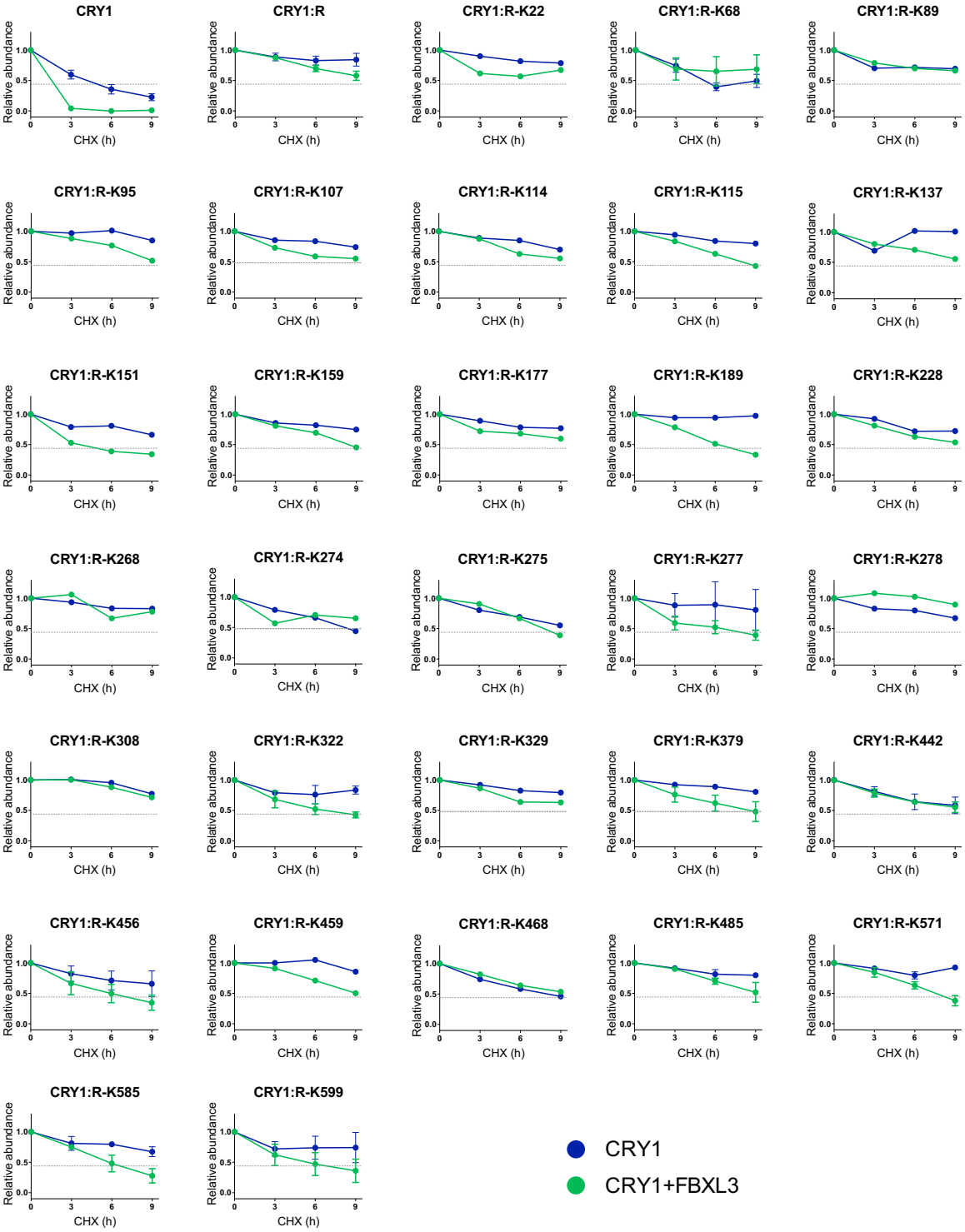

Figure S6. CRY1 Lysine Site Mapping for FBXL3-Mediated Degradation, Related to Figure 7 and Table S2

Quantitative measurement of degradation of individual revertants. *Cry1* constructs were transfected alone or with *Fbxl3* (50ng *Cry1* construct / 35ng *Fbxl3* construct) into 293A cells. Cells were treated with CHX (100ug) and sampled after 0, 3, 6, or 9 hr. Data are mean ± SEM (error bars shown when n = 3 or more). The initial screen in the presence of FBXL3 resulted in 6 candidate lysines (K68, K189, K277, K456, K585, K599), in addition to the 4 candidates found in the forward mutagenesis screen (K107, K228, K159, K308). Candidate residues were chosen based on CRY1 half-life in the presence of FBXL3 as well as rate of degradation. The K68 residue was included because it caused overall instability of the protein, whereas K151 residue was excluded from further analyses due to inconsistent degradation patterns in independent experiments.

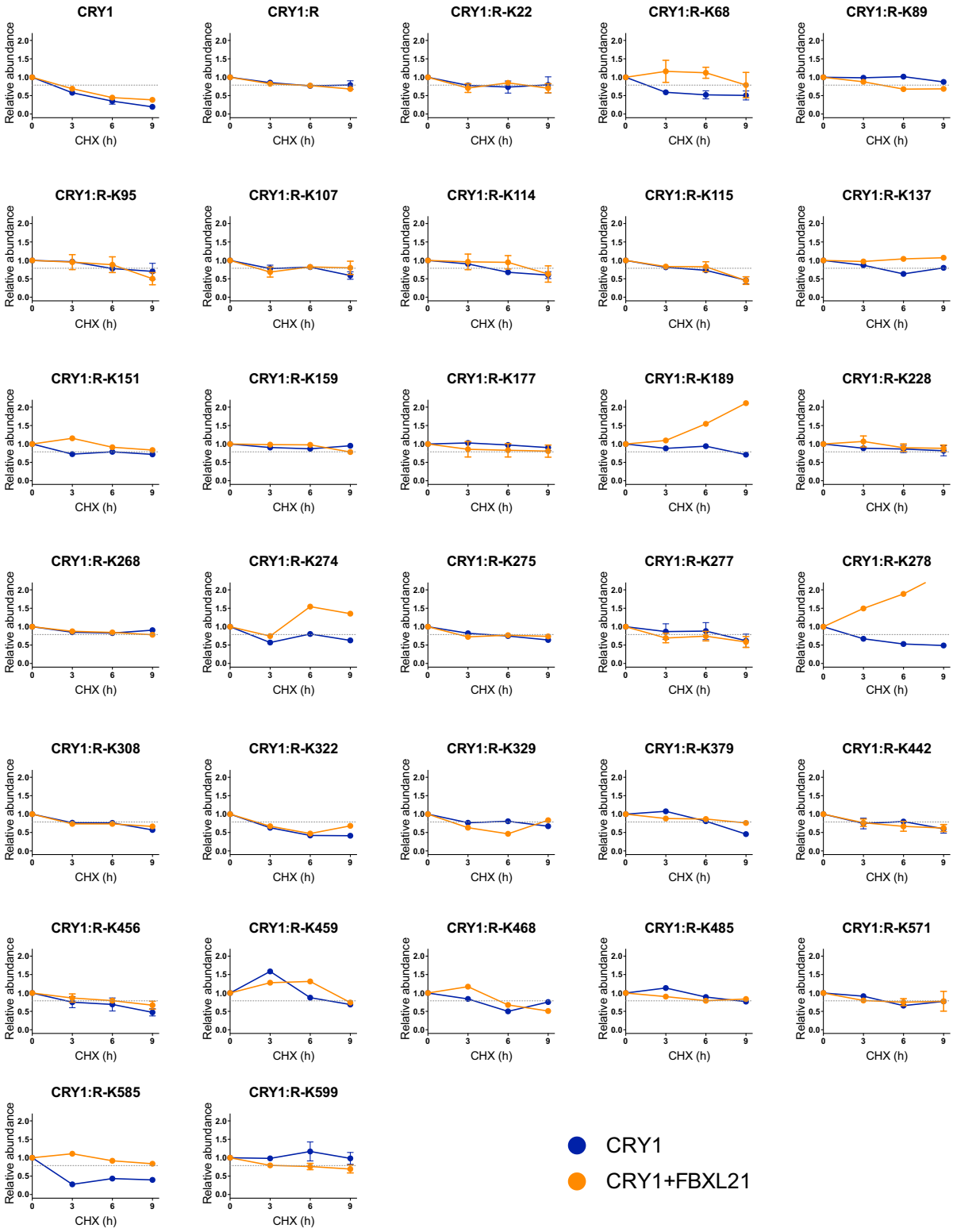

Figure S7. CRY1 Lysine Site Mapping for FBXL21-Mediated Degradation, Related to Figure 7, Table S2

Quantitative measurement of degradation of individual revertants. *Cry1* constructs were transfected alone or with *Fbxl21* (50ng *Cry1* construct / 35ng *Fbxl21* construct) into 293A cells. Cells were treated with CHX (100ug) and sampled after 0, 3, 6, or 9 hr. Screen for degradation in the presence of FBXL21 resulted in no obvious candidates other than the moderate degron candidate K11 (Figure 7E). Data are mean ± SEM (error bars shown when n = 3 or more).